2015

Autogenous Welding on a Flat Plate: The Effect of Phase Change Transformation on Residual Stress

Bin Yang
Lehigh University

Autogenous Welding on a Flat Plate: The Effect of Phase Change Transformation on Residual Stress

by

Bin Yang

Presented to the Graduate and Research Committee

of Lehigh University

in Candidacy for the Degree of

Master of Science

in

Mechanical Engineering

Lehigh University

2014

This thesis is accepted and approved in partial fulfillment of the requirements for the Master of Science.

_____

Date

_____

Thesis Advisor

_____

Chairperson of Department

Acknowledgment

The encouragement and advice I received while writing this thesis from Professor Herman F. Nied must be gratefully acknowledged. Professor Herman F. Nied gave me much support and constructive comments on my research and thesis. In addition, I gratefully thank Muhammed Ashraf, Xiao Liu, and Tianyi Luo for helping me with access to the workstation.

Also, I express my love to my parents and sister.

Table of Contents

List of Figures

List of Tables

Abstract

The objective of this study is to predict the magnitude and spatial variation of the residual stresses in an autogenously welded flat plate. Autogenous welding is a fusion welding process using heat without the addition of filler metal to join two pieces of the same metal. The residual stresses in a flat plate, close to the weld pool, are closely examined in this study. Using the welding simulation program SYSWELD, a 2-D geometric model was constructed using ANSYS 15.0, then meshed with quadratic 2-D elements in Visual-Mesh 10.0. In this study, mesh refinement is critical, especially near the melt boundary, so that realistic results can be obtained where the thermal and material property gradients are most severe. In the welding simulations, material properties for 316L austenitic stainless steel and S355J2G3 carbon steel are chosen to contrast the difference in residual stresses obtained from two very different classes of steel. In addition, results are given for three different boundary conditions. It is shown that the material properties and boundary conditions have a significant influence on the residual stresses. Of particular interest is the comparison of the final residual stresses. It is shown that the phase change transformations during cooling in carbon steels from austenite to bainite and finally martensite, result in highly localized compressive residual stresses, significantly reducing the magnitude of the overall surface tensile stresses in the heat affected zone near the weld boundary.

Chapter 1. Introduction

1.1 Background

It is commonly recognized that fusion welding generates residual stresses that can play an important role in structural reliability. In general, welding residual stresses are introduced as a consequence of local thermal gradients and plastic deformations created by rapid heating and subsequent cooling of a moving heat source. Knowledge of the residual stress field is of importance for the functional design of the structure, as it will influence the mechanical behavior of a structure in several ways. For example, high tensile residual stresses may lead to premature cracking. During the welding process, the combined thermal stresses and the phase transformation stresses will invariably exceed the material's yield strength, so that after cooling, there will be large internal stresses and measurable welding induced distortions which cannot be eliminated. The macroscopic stress in the weldment after cooling depends on the welding process parameters, the high-temperature material properties, and the clamping conditions during the welding process. The welding stresses and metallurgical transformations are strongly dependent on the non-uniform temperature field introduced during the welding process.

Welding residual stresses have a critical influence on a variety of applications. The welding residual stresses will influence the fatigue life of a load bearing structure, the structure's stiffness, and the structure's ultimate strength. The influence of residual stresses on fatigue life has been studied numerically by modelling the residual stress field after welding with different levels of accuracy [1].

The residual stress due to welding, can be considered as the initial stress state which exists on the unloaded component. During a component's service, the welding residual stress and the working stress are superimposed. The combined stresses may alter the stiffness and stability of the structure. In addition, under the combined effects of temperature and alternating loads, welding residual stresses may seriously affect fatigue life. The resistance to brittle fracture, the ability of the structure to resist stress corrosion cracking, and high temperature creep cracking, can also be adversely affected by welding residual stresses [2].

When the superposed stresses caused by external loading and the welding residual stresses exceeds the material's yield point, the structure will plastically deform, and in certain cases, lose the ability to further withstand increasing external loads. Longitudinal and transverse welding lines on a structure, such as the weld line on a ribbed plate or an I-beam, will create high tensile residual stresses at the weld, which will introduce compressive stresses in the bulk of the component away from the weld. Although the residual tensile stress is not very big in the distribution of the length of the component, it will bring a greater impact on the component.

If the welded component is fabricated from a relatively brittle material, or is constrained in a manner that severely restricts plastic deformation, as the increasing external loads, stresses of the component cannot be uniform. The peak stress will continue to increase until it reaches the yield limit of the material. Then it will create a local failure that may eventually lead to fracture of the entire component. Residual stresses due to welding will usually decrease the ultimate load carrying capacity of a structure, often leading to the fracture close to the weld when failure occurs. For material subjected to large

triaxial constraint, which hinders the generation of plastic deformation, there can be a significant reduction in the apparent ductility of the component. [3]

A component's residual stresses can be superposed with the stresses caused by external loading. When the superposed stresses reach, or exceed, the yield limit of the material, the cross-section with the residual tensile stress will advance into the plastic zone, then the increasing external load is shifted to the remaining elastic zone of the cross-section. For sufficiently ductile materials, with increasing load, the elastic zone will decrease and the plastic zone will increase. Then the internal stress will continue to superimpose and the stress will redistribute until the stress of the entire cross-section reaches the yield limit. However, the plastic material will lose the effect of constraint under the certain condition, or the plasticity of the component will be very low and residual stress will impact on the static stiffness. In the loading process the peak stress will continue to increase until it reaches the limit of the strength of the material and the component is damaged, because of that the component will not generate the sufficient plastic deformation.

It is well known that phase transformations have a significant influence on the welding residual stresses, especially for carbon steels. Carbon steel passes through a series of the metallurgical phase changes: ferrite, pearlite, austenite, bainite, and martensite, when heated and cooled [4]. When the temperature of carbon steel is higher than the eutectoid temperature during heating, the components of the pearlite or austenite-martensite will quickly transforms to austenite. During the cooling process of carbon steel, the austenite will transform to pearlite, bainite, and finally martensite, at a rate depending on the temperature, cooling rate and local stress state [5]. The local material properties will change

according to these phase transformations, which are known to introduce local volumetric strains. In addition, the state of the stress and yield strength can be strongly affected by the volumetric strains, e.g., transformation plasticity. This study focuses on how the residual stresses are influenced by these phase changes. Of particular interest is the stress state at the melt boundary, where within a very narrow zone phase changes can radically alter the local stresses and have a significant impact on subsequent fatigue failure behavior.

1.2 Welding simulation of an autogenous weld in a flat plate

Autogenous welding is a process by which, through the use of a fusion heat source, the edges of metal parts, placed against each other, are heated to their melting point so they fuse. After the welding and cooling, the parts form one body of almost the same physical properties [6]. In this study simulation of autogenous welding along a symmetric bond line is chosen so that a single set of temperature dependent material properties can be used throughout the simulation. This avoids the introduction of any stress singularities due to a discontinuity in material properties between the filler metal and the base alloy. In addition, since there are no geometry changes due to the addition of a weld bead, stress concentrations at the toe of the weld are completely avoided.

Residual stress measurements are most readily carried out on the surface of a component at start of life or after service duty. The techniques commonly used for these measurements include X-ray diffraction and various hole-drilling techniques [1]. It is bery useful to be able to determine the welding residual stresses using both experimental techniques and computational methods. The experimental measurement of the welding residual stress is not always feasible, although it should be utilized as validation for analytical and numerical studies. Nevertheless, finite element systems are used increasingly to simulate material response and the evolution of residual stresses during welding [7].

There exist several commercial finite element codes that may be employed for detailed nonlinear simulations of the development of the temperature and stress fields

during welding processes. In this study, the welding residual stress predictions were made using the SYSWELD [8] finite element software.

Resulting from more than 20 years of development, SYSWELD is a leading tool for the simulation of heat treatment, welding and welding assembly processes, taking into account numerous aspects of material behavior, design and process [9]. SYSWELD performs non-linear computations with all material properties dependent on temperature, phases/material transformations, proportion of chemical elements, and auxiliary variables. In addition, SYSWELD covers most dominant non-linear phenomena, such as non-linear heat transfer, non-linear geometries including large strains, isotropic and kinematic strain hardening, in addition to phase transformations, transformation plasticity, and non-linear mixture rules for the yield stress of phases [10].

This study also utilized SYSWELD's newest visual interface, Visual-Environment 10.0 (Figure 1.1), which is a single integrated graphical user environment. It includes a comprehensive modeling tool to generate meshes on complex geometries for various engineering domains. Visual-Environment's interactive post-processing module is also very effective for displaying temperature/stress/phases, etc., graphically.

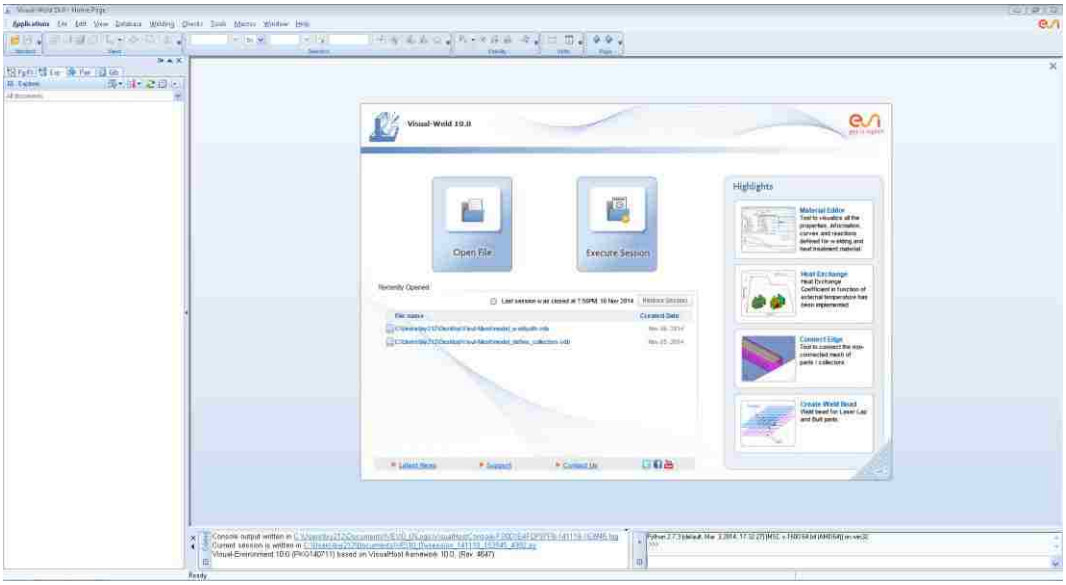

Figure 1.1 SYSWELD's Visual-Weld 10.0 graphical interface running in Windows

In the Visual-Environment package, Visual-Mesh is used for creating the geometry and mesh files. Visual-Mesh can be used to automate surface clean up, mid-surface creation and meshing, and generally provides an intuitive guided mesh process. [11]

Visual-Viewer, a subset of the Visual-Environment software, is a workflow-based user interface for modeling welding fabrication processes. [12]

The Visual-Viewer module is a complete post processing environment for output from SYSWELD. Visual-Viewer allows easy and fast graphical interpretation with very useful animation control features such as simple section cut tool, video reading and aligning with simulations, synchronized simulation, and plot windows (Figure 1.2).

Visual-Mesh, Visual-Weld, and Visual-Viewer cover the three main phases of welding simulation starting from interfacing with CAD formats, CAD cleanup, meshing, model set-up, post-processing using one single data model (Figure 1.3).

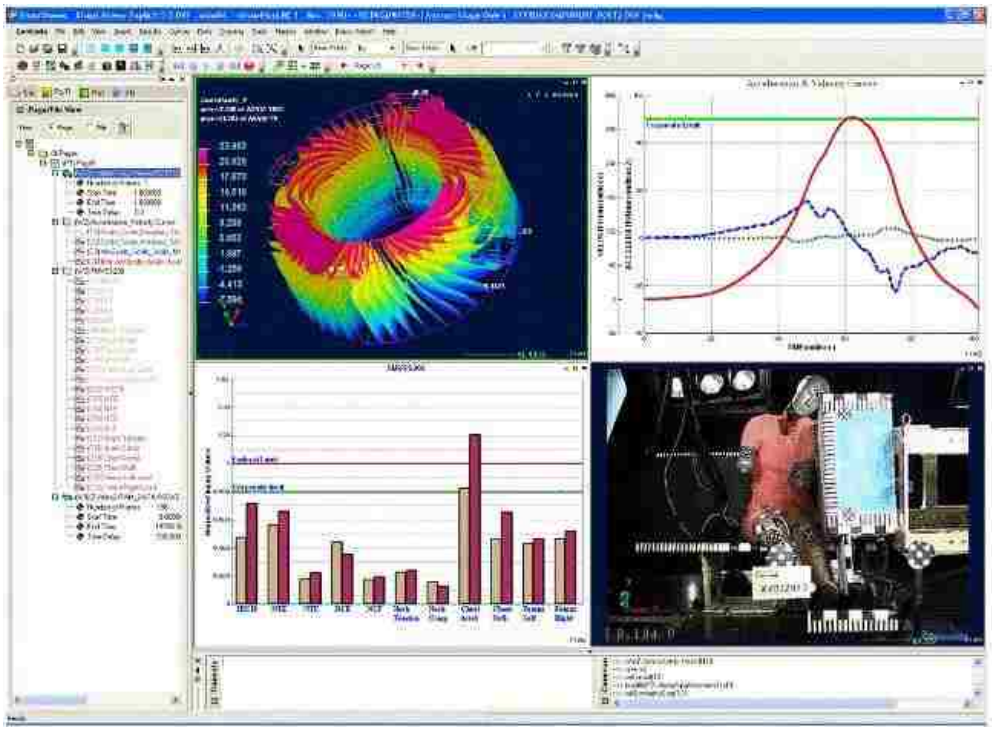

Figure 1.2 Results presented by Visual-Viewer [13]

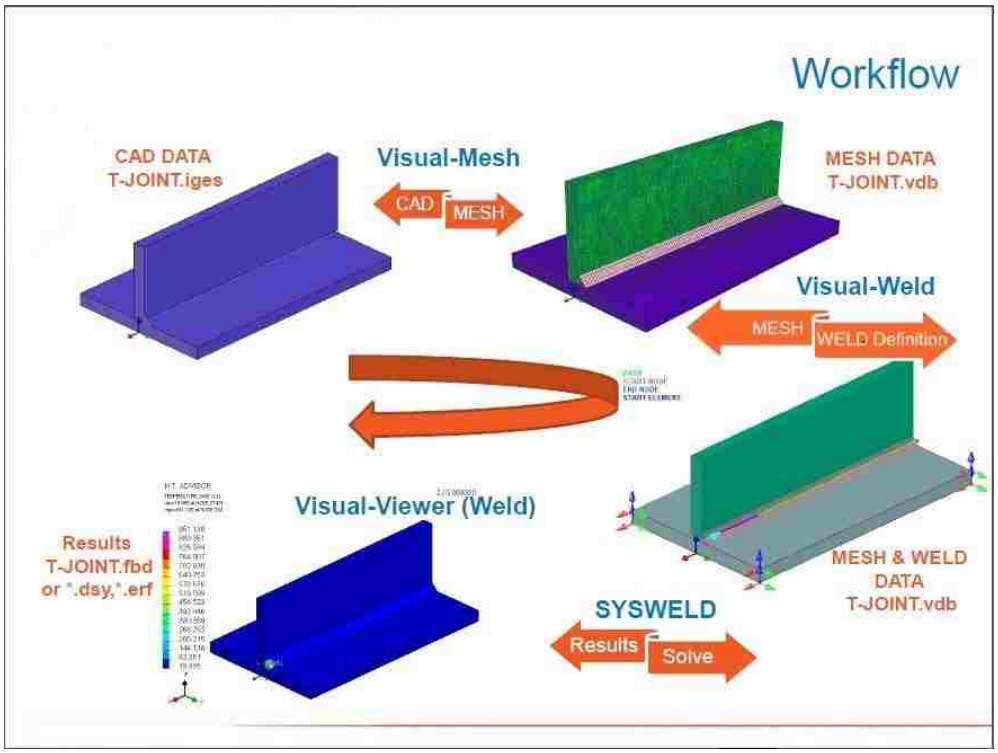

Figure 1.3 Workflow of simulation with Visual-Environment [14]

Chapter 2. Welding model

2.1 Basic 2-D geometric model

The dimensions for the flat plate used in this study are shown schematically in Figue 2.1. The flat plate was welded using heat without the addition of filler metal in the middle of the top surface, i.e., a zone of metal along the plane of symmetry was melted and cooled by the moving heat source. Of particular interest, is the cross-sectional view of the welded flat plate shown in Figure 2.2. The penetration depth of the weld and outline of the heat affected zone indicates that as the welding heat source proceeds in a linear path, the melting in the cross-section generally takes the shape of a semi-circular zone.

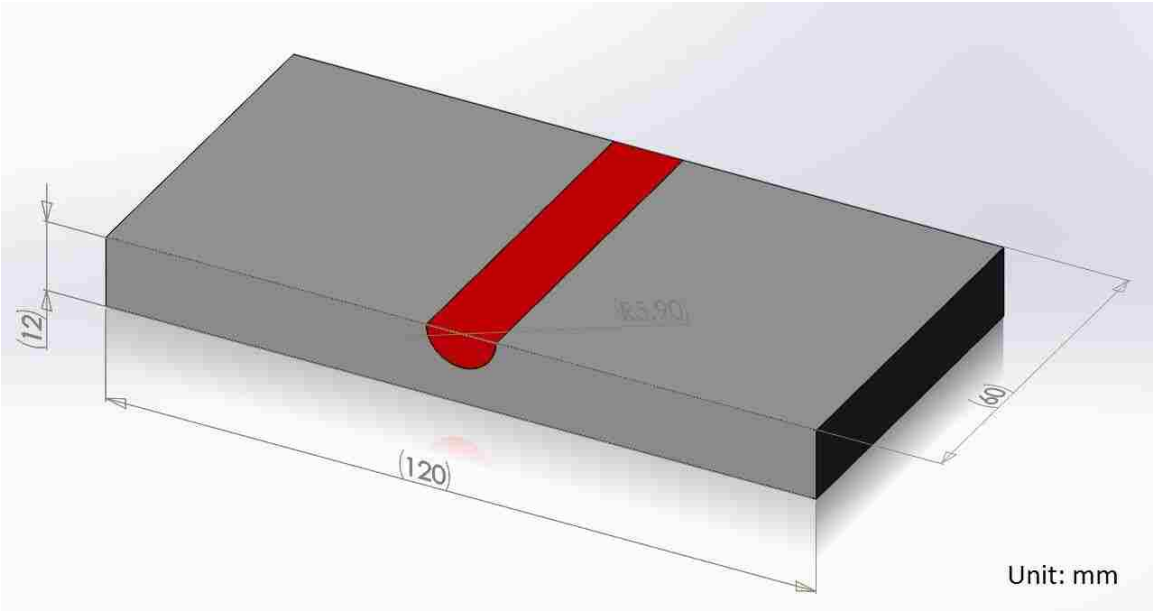

Figure 2.1 Dimensions of flat plate

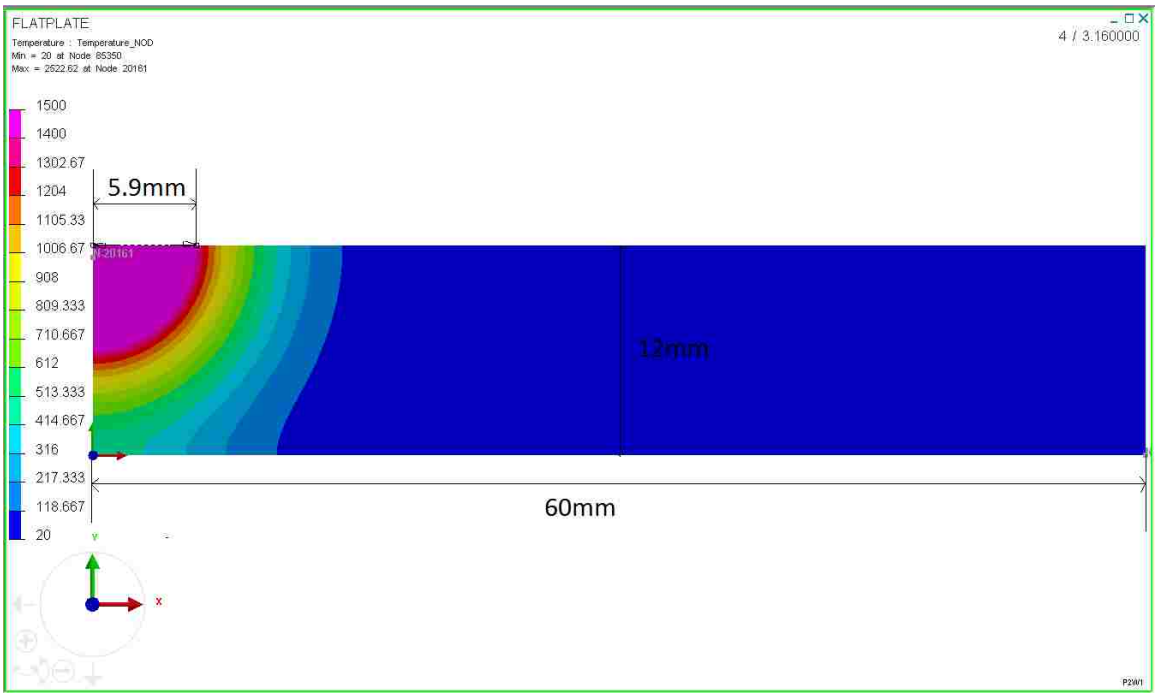

Figure 2.2 Cross-sectional view of temperature contours in the flat plate

When constructing the model for the welding simulation, one of the first and most significant determinations to be made is whether the model will be created in two or three dimensions. The welding simulations with two and three dimensions both have certain advantages and disadvantages. The most considerable advantage of the two-dimensional model is decreased computation time. It is also easier to construct and manipulate graphically. Fewer time steps are usually required as the welding source only affects the modeling plane. Once the welding simulation has finished, the 2-D solutions and results of the simulations are also more easily rendered visually and understood.

In this study, the 2-D geometric model of the flat plate was constructed using ANSYS 15.0 [15]. The resulting file was then exported in the ".IGES" format. When Visual-Mesh 10.0 splits the surface into small pieces, it will generate some irregular surfaces which cannot be meshed uniformly. The benefit using ANSYS 15.0, is that it makes it possible to

split the surface into small pieces that are regular and uniform. Near the melt boundary, where the local stresses and material phase transformations have a steep gradient, a smoothly refined mesh is highly desirable. In order to get a sufficiently refined and uniform mesh around point “a” in Figure 2.3, the surface around this point is split into a number of smaller surfaces (the yellow surface in Figure 2.3).

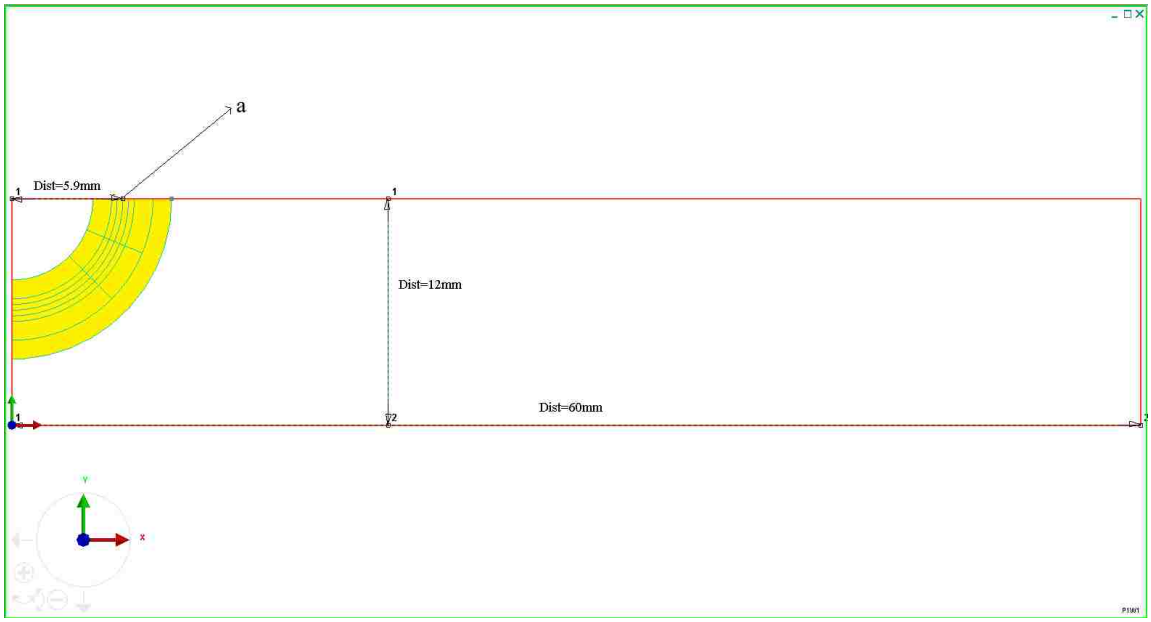

Figure 2.3 2-D geometric model of flat plate

2.2 Meshing

The geometric model that was created using ANSYS 15.0, was then imported into the Visual-Environment, i.e., Visual-Mesh 10.0. During meshing of the model, the element size near the point "a" is specified to be 0.02mm in order to ensure that the local mesh in this region is very small. In this study, the element's type is specified to be "Quad" and the element's order is "Linear", i.e., four-noded quadrilateral and three-noded triangles were used. If the element's order is set to be "Quadratic", this will greatly increase the number of degrees of freedom and it was generally found that with this level of mesh refinement the additional degrees of freedom were unnecessary. Figure 2.4 shows the distribution of residual stresses on the top surface of the flat plate for 316L austenitic stainless steel under the unclamped boundary condition during the entire welding process. The values of σ_{yy} and σ_{xy} on the plate's surface are very close to zero, satisfying the traction stress-free boundary condition. The meshes for the finite element models used in this study are high refined, so when checking for coincident nodes, it was important to specify the value of the max gap in the detection to be very small (Figure 2.5), otherwise the automatic meshing algorithm will produce too many coincident nodes for the surfaces near point "a". Figure 2.6 shows the final finite element model for the flat plate with a highly refined mesh suitable for detailed stress analysis at the weld boundary.

Figure 2.4 Residual stresses on the top surface of flat plate

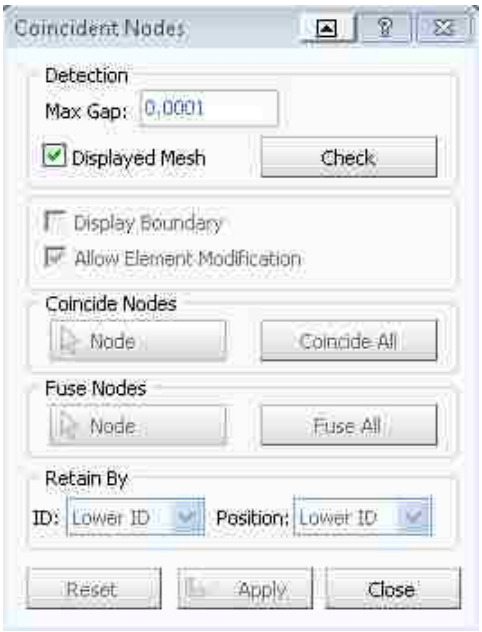

Figure 2.5 Window of checking coincident nodes

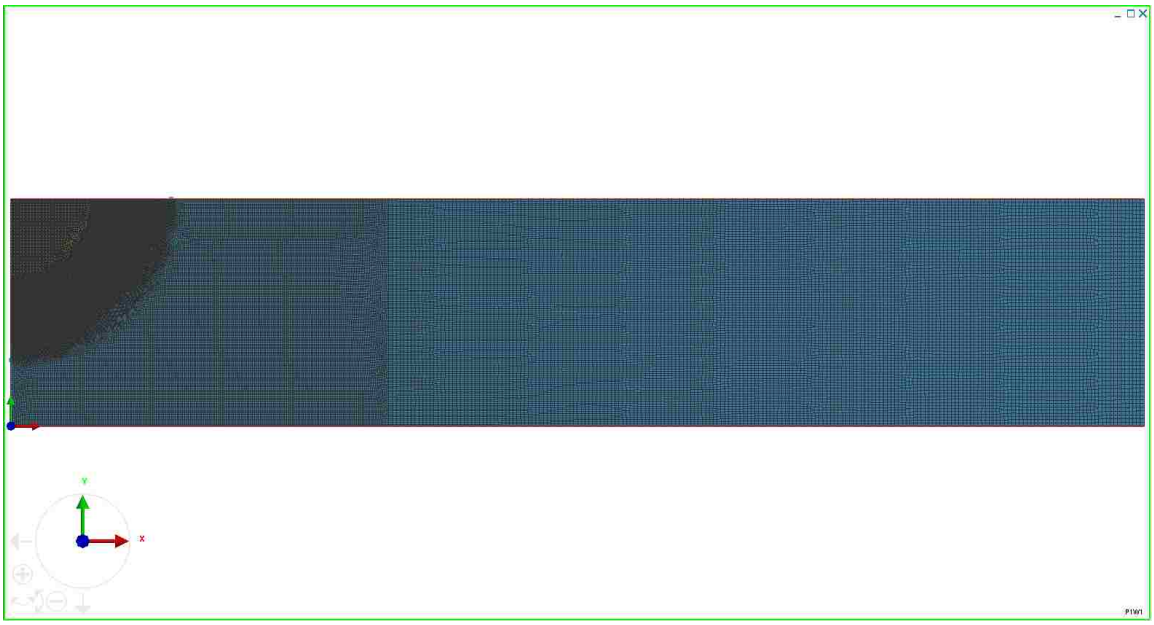

Figure 2.6 Final finite element model of flat plate

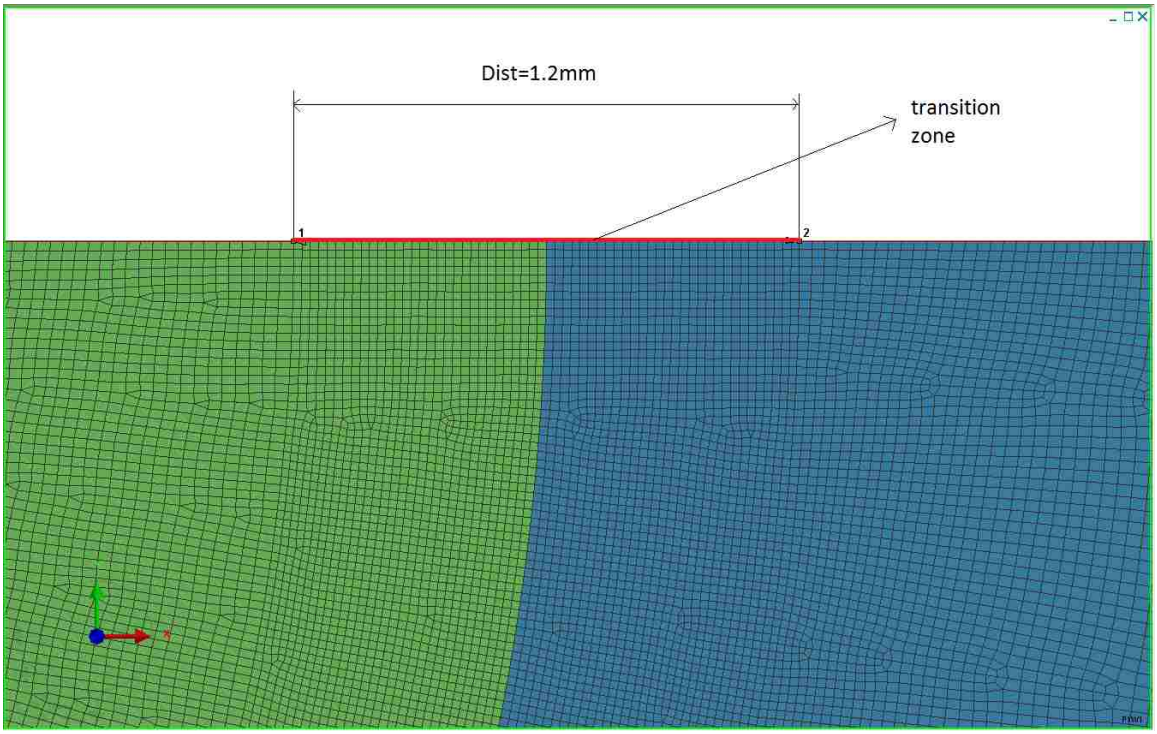

Figure 2.7 Detailed meshes near melting zone

The number of the “Quad” elements in this highly refined model is 97436, and the number of the “Triangular” elements is 350, so there are a total of 97786 2-D elements in the finite element model for the flat plate. There are 98243 nodes and the number of the nodes on the top surface of the flat plate is 548. Figure 2.7 shows a close-up of the refined mesh in the “narrow” transition zone between the melt pool and the solid plate. In about 1.2mm, there are 60 2-D elements with 61 nodes on the top surface near the melt boundary.

2.3 Welding model

Figure 2.8 shows the dialog box used to define the "load" of the welding heat source. This is done by selecting all the elements in the welding zone (the highlight yellow elements in Figure 2.8), then adding them into a new collector with the name "J01_LOAD". These elements are significantly affected by the moving heat source during the welding process.

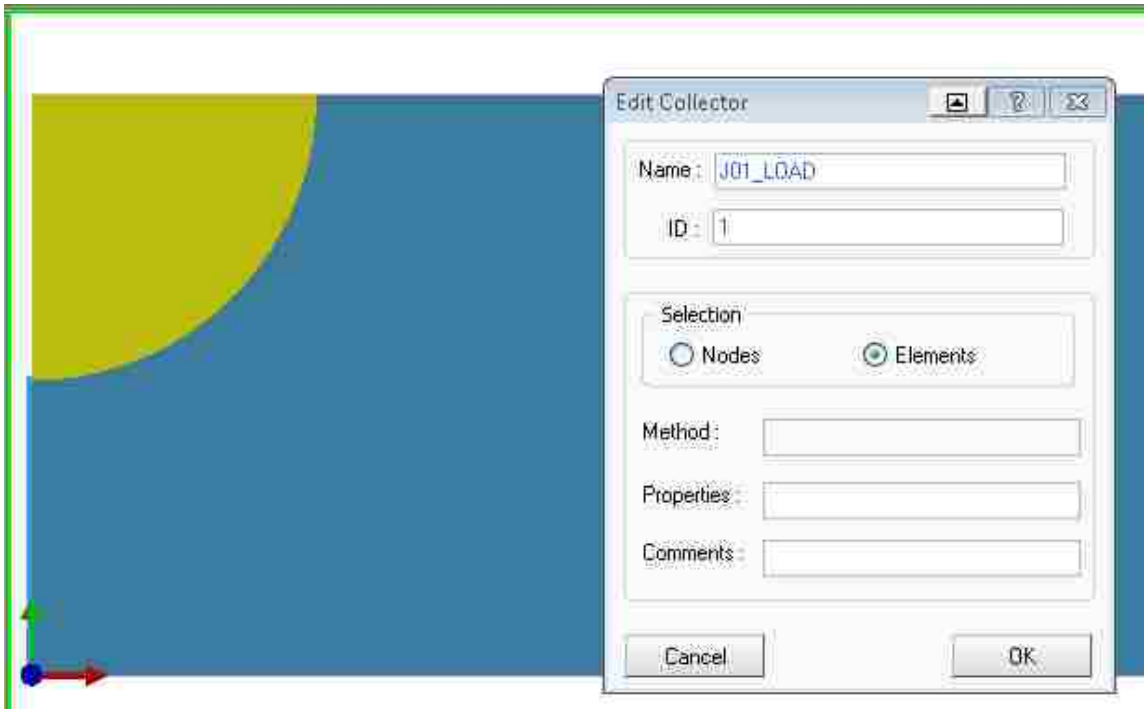

Figure 2.8 Defining load of welding model

In this study, define three additional collectors are created, which contain the clamping conditions are also created. These collectors consisted of the nodes (highlighted in Figure 2.9). The boundary condition collector, designated as "RIGID01_CLAMP", contains all but the first bottom node on the vertical line along the plane of symmetry. The second collector, named "RIGID02_CLAMP", contains all but the first node on the bottom

of the flat plate. The third collector, named “RIGID03_CLAMP”, contains the single corner node on the vertex where the horizontal and vertical edges of the model meet.

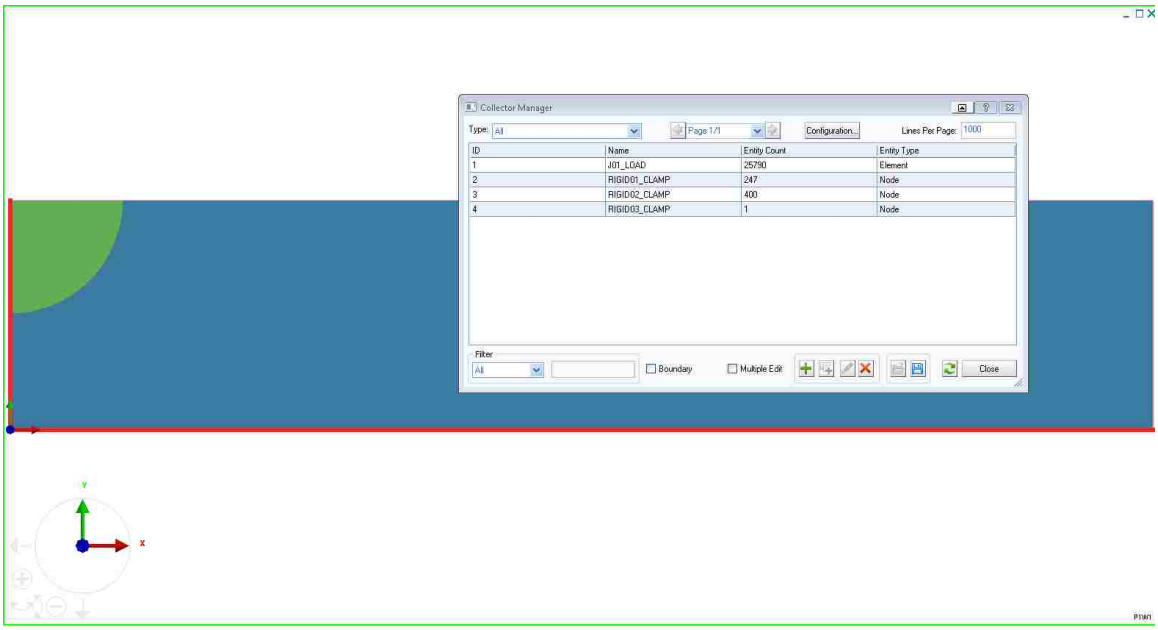

Figure 2.9 Defining collectors for the clamping boundary conditions

The welding path is defined in the Visual-Weld module. This is shown in the window “Create Trajectory” (Figure 2.10), where node 1 is used to represent the weld line and node 2 a reference line. The heat source follows the weld line and uses the reference line for angular orientation with respect to the weld line. Figure 2.11 shows the final welding model, with the center of the weld line located at the plate surface on the plane of symmetry.

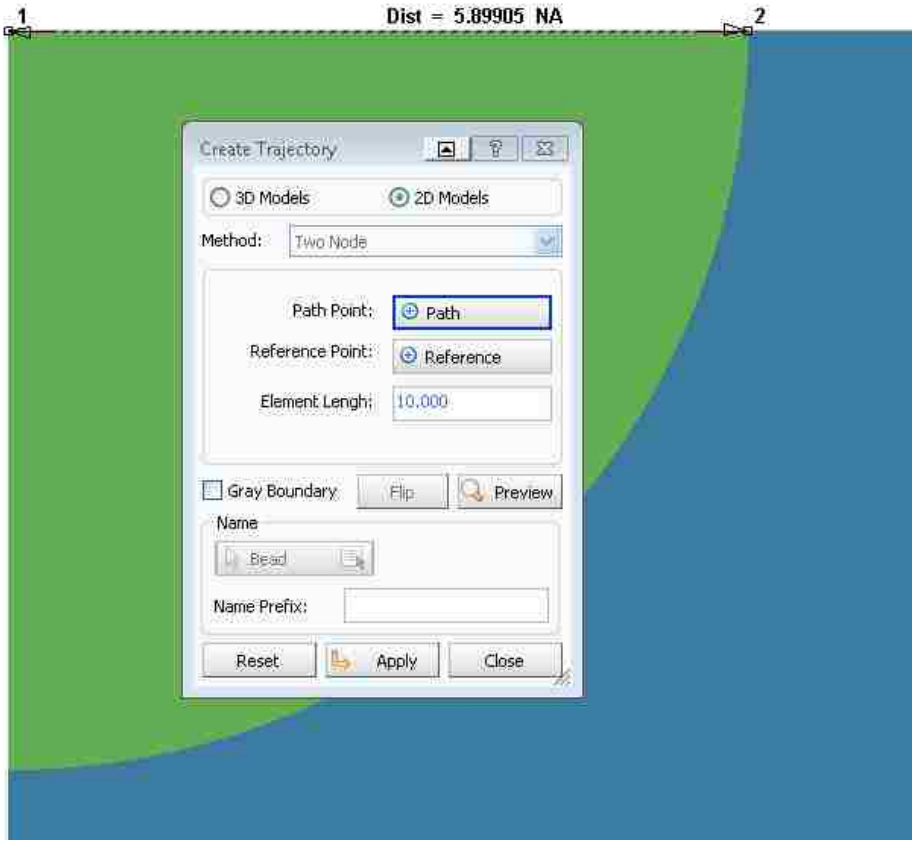

Figure 2.10 Defining welding path

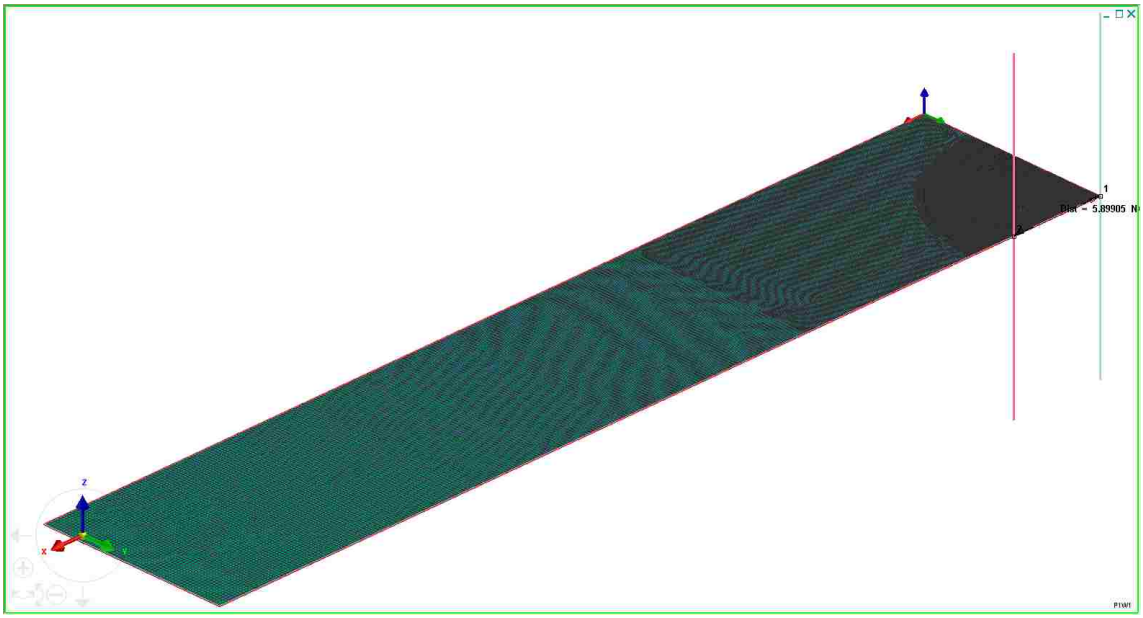

Figure 2.11 Final Welding model

Chapter 3. Welding Simulation

3.1 Materials

In the welding simulations, two material properties are separately used: 316L austenitic stainless steel, and S355 carbon steel.

The 316L austenitic stainless steel has a homogenous austenitic structure at room temperature. Austenitic stainless steel has no magnetism, and excellent toughness and ductility. However, the yield strength of 316L austenitic stainless steel is relatively low, and it cannot be strengthened by the phase transformation. The only way to improve the strength of the austenitic stainless steel is by cold working. [16]

Austenitic stainless steels are generally considered to be the most weldable of the stainless steels and can be divided rather loosely into three groups: common, chromium-nickel (300 series), manganese-chromium-nickel nitrogen (200 series) and specialty alloys [17]. Austenitic is the most popular stainless steel group and is used for numerous industrial and consumer applications, such as in chemical plants, power plants, food processing and dairy equipment. Austenitic stainless steels have a face-centered cubic structure. Though generally very weldable, some grades can be prone to sensitization of the weld heat-affected zone and weld metal hot cracking.

Table 3.1 Chemical composition of 316L austenitic stainless steel

Grade	%Cr	%Ni	%C	%Mn	%Si	%P	%S	%N	%Mo
316L	16-18	10-14	0.03	2	0.75	0.045	0.03	0.1	2.0-3.0

The S355 is considered to be a standard grade structural steel and is formed in a range of industry standard cross-sectional shapes. The structural steel grades are designed with specific chemical compositions and mechanical properties formulated for particular applications.

Structural steels are used in many load bearing application. They are particularly useful because they offer the unique combination of good welding properties with guaranteed strengths. S355J2G3 is a low carbon, high strength, and carbon manganese structural steel. With its low carbon content, it possesses good cold-forming properties.

Table 3.2 Chemical composition of S355J2G3 carbon steel

Chemical elements	C max	Si max	Mn max	P max	S max	Cr max	Mo max	Ni max	Al min
% by mass	0.22	0.55	1.6	0.035	0.035	0.03	0.08	0.3	0.02
Permissible deviation	+0.02	+0.03	+0.04	+0.005	+0.005	+0.05	+0.03	+0.05	-0.005

3.2 Defining the welding simulation with Visual-Weld 10.0

In the Visual-Weld 10.0 application, welding process parameters are specified after importing the welding finite element mesh. In the Visual-Weld 10.0 main menu, “Welding” is selected to open the “Welding Advisor” window.

The first step, “Project Description”, is where the project details can be specified, such as name, title, working directory, general description and material description (Figure 3.1).

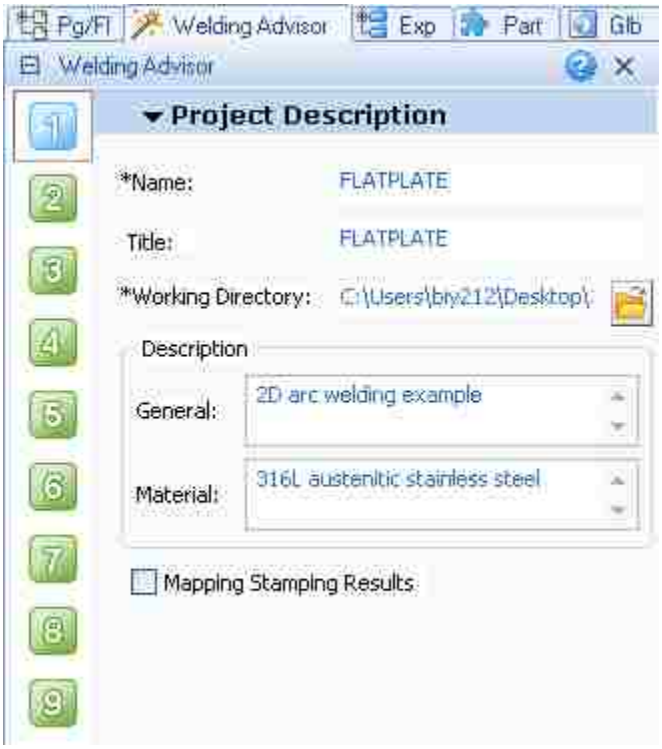

Figure 3.1 Setting up project details

In step 2, “Global Parameter”, the “2D Cross Section” should be selected (Figure 3.2). Based on the mesh of the finite element model, the welding advisor will set up the computation option automatically. However, in this study the “2D Cross Section” selected to obtain the two-dimensional generalized plane strain solution.

Figure 3.2 Defining global parameter

In step 3, "Component Properties", are used to set up the material properties (Figure 3.3). For this welding simulation, the materials, 316L or S355J2G3, can be found in the SYSWELD database in the pull down menu "Material".

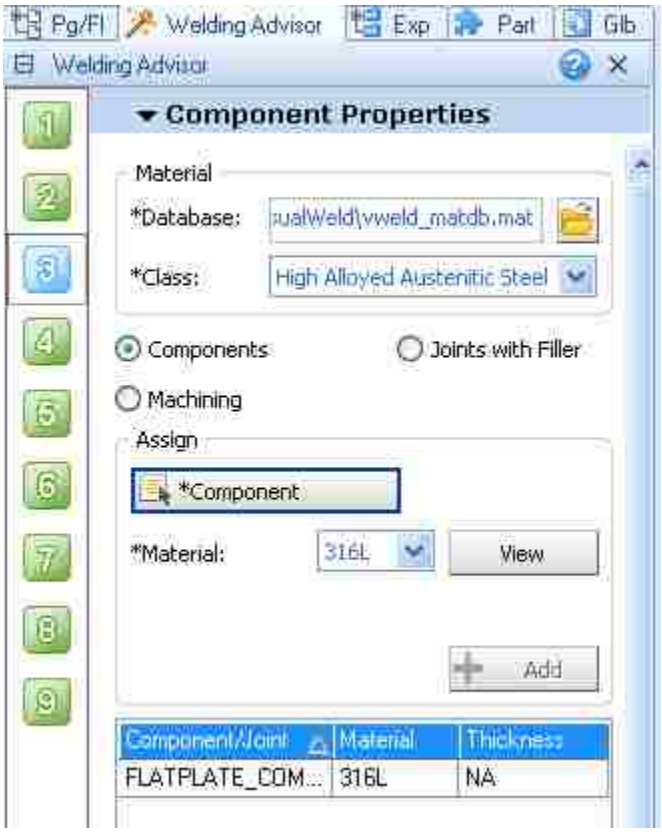

Figure 3.3 Setting up materials of components and joints

In step 4, “Welding Process”, the welding parameters can be defined. Set the process type to be general arc, energy/unit length of weld in J/mm, and velocity in mm/sec. The parameters for the weld pool can be defined as shown in Figure 3.4. In the pull down menu of “Energy”, the “Energy/Unit length” should be defined carefully. For 316L austenitic stainless steel, in order to make the temperature in the welding zone greater than the melt temperature of ~1400℃, the value of the “Energy/Unit length” should be 515 J/m. This value needs to be obtained by trial and error to ensure the desired weld shape. For S355J2G3 carbon steel, the “Energy/Unit length” for S355J2G3 was determined to be 600J/mm. This is an energy density sufficient for producing temperatures in the melt that exceed the ~1500℃ melting temperature for S355J2G3. Thus, in the subsequent welding simulations a greater heat input was used for the S355J2G3 than the 316L to obtain the same size welds.

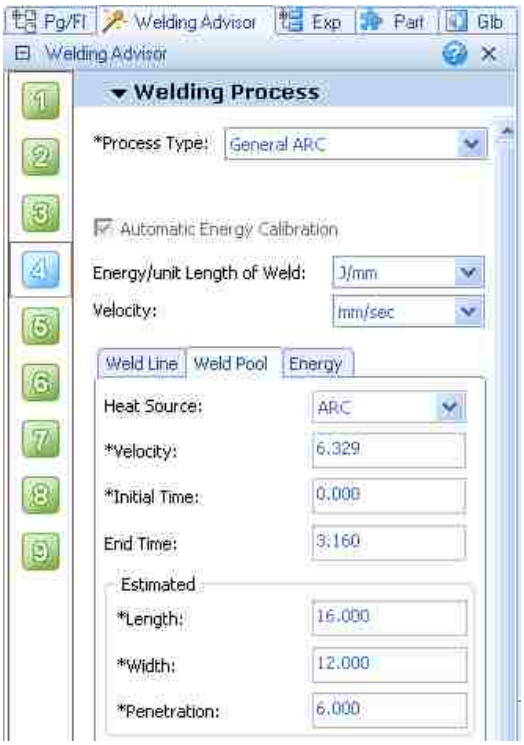

Figure 3.4 Defining welding process

In step 5, “Cooling Condition”, the cooling boundary condition can be defined (Figure 3.5). The “Medium” was specified to be “Free Air Cooling”, the “Ambient Temp” to be 20℃ and the “End Time” to be 3600s.

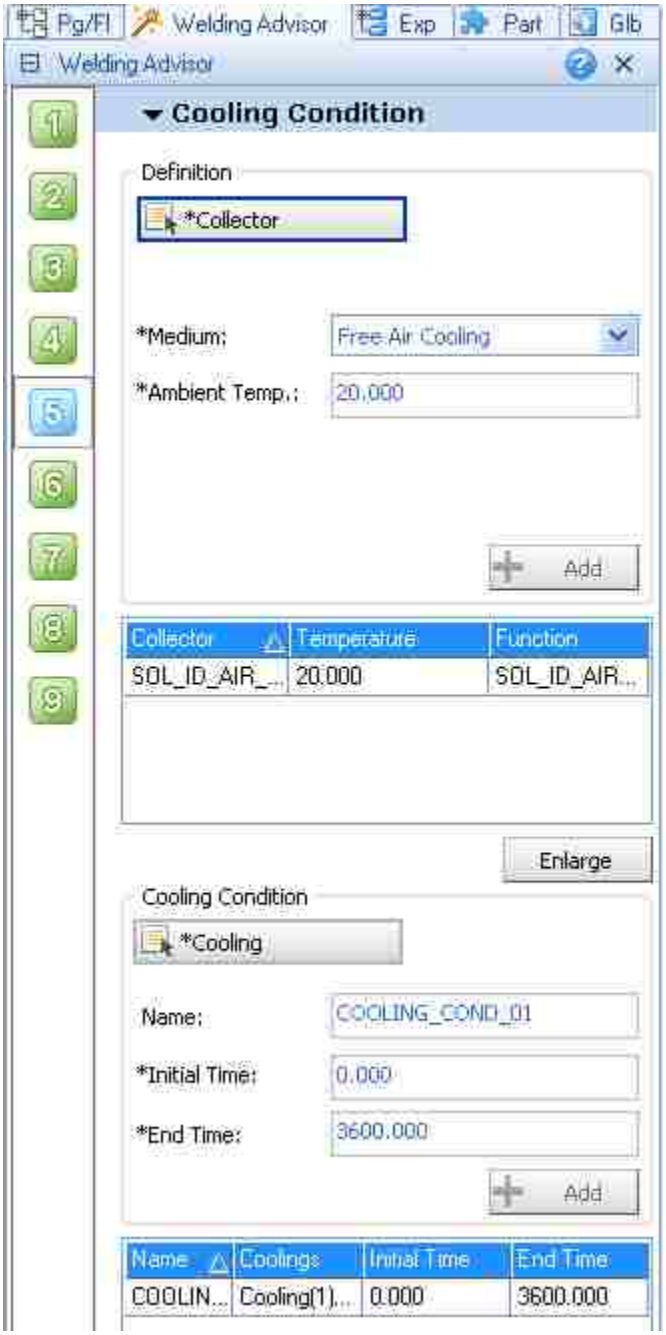

Figure 3.5 Setting up cooling boundary condition

In step 6, “Clamping Condition”, the boundary conditions were set as shown in Figure 3.6.

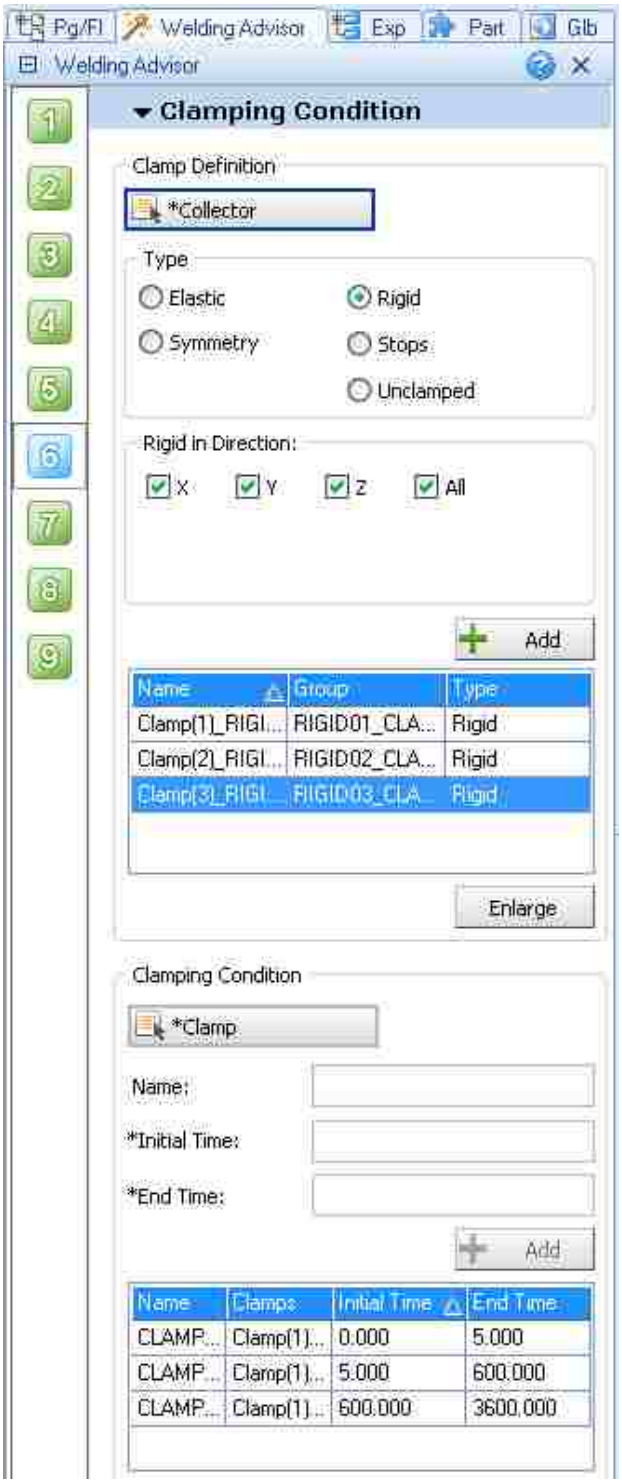

Figure 3.6 Defining boundary conditions

There are three boundary conditions for the flat plate model in this study. Boundary condition 1 is shown in Figure 3.7(c): all but the first bottom node on the vertical line is restrained in the X-direction during the heating and cooling process (Figure 3.7(a)), then set the single corner node on the vertex where the horizontal bottom and vertical left edges of the model meet to be restrained in all directions in the heating and cooling process (Figure 3,7(b)).

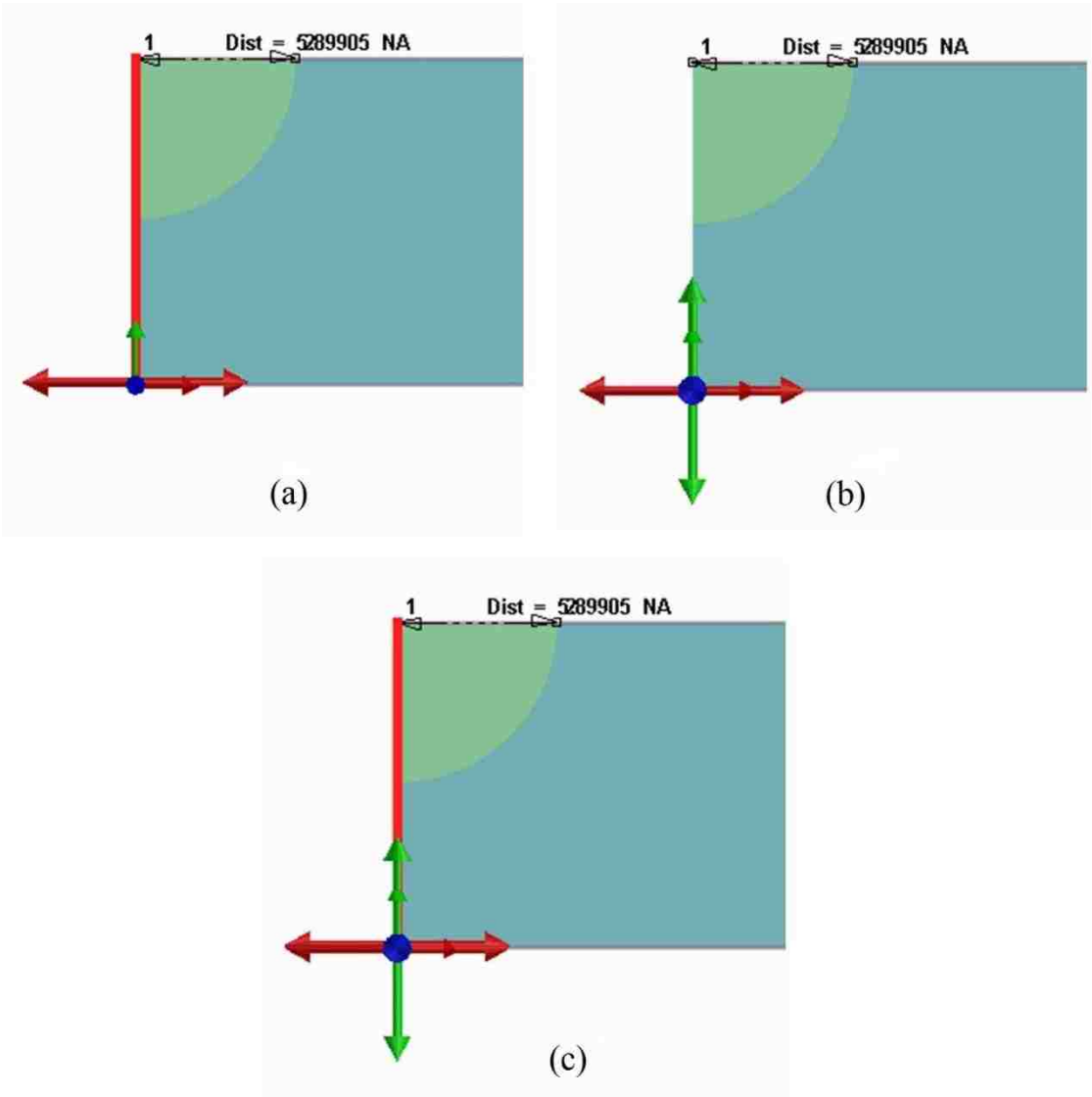

Figure 3.7 Unclamped condition during the entire welding process

Boundary condition 2 (Figure 3.8(b)): include the boundary condition 1 and there is another one. Set all but the first node on the bottom of the flat plate model to be restrained in Y-direction in the heating and cooling process (Figure 3.8(a)).

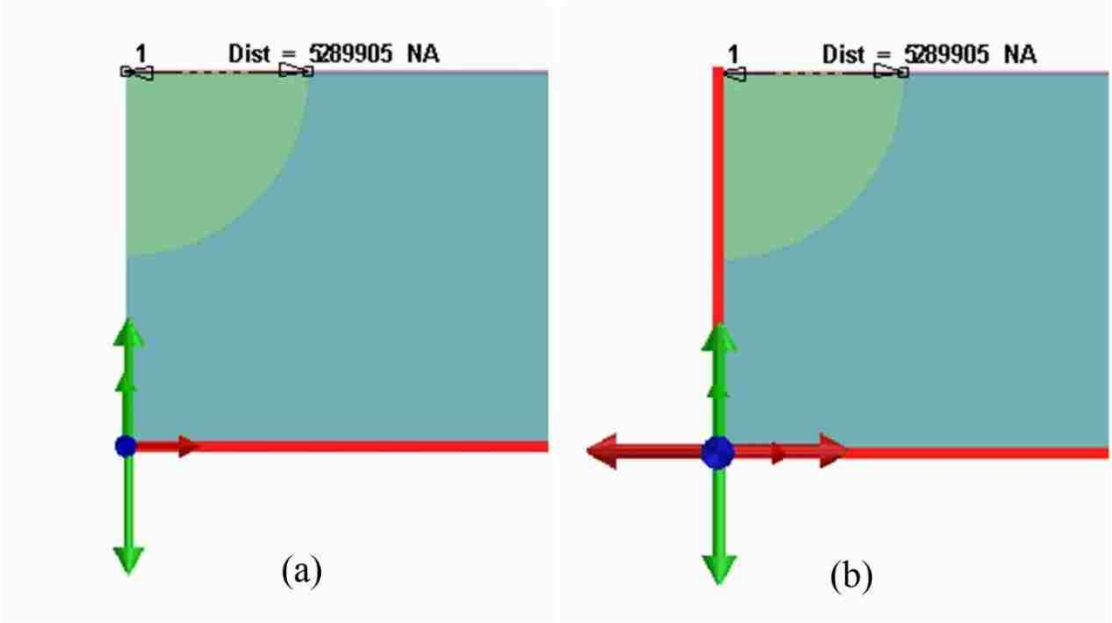

Figure 3.8 Before release of clamped condition

Boundary condition 3 (Figure 3.9): include the boundary condition2, but after cooling release the boundary condition on the bottom.

Figure 3.9 After release of clamped condition

For step 7, “Loads and Deformations”, and step 8, “Contact Definition”, this study does not include any external loading conditions and contact conditions. So there is no actions in these steps.

In step 9, “Solution Parameter”, the “Mechanical” should be toggled on and the “Initial Temperature” should be 20℃. Then select the “Generate Input Data” to export all the projects files in the working directory (Figure 3.10).

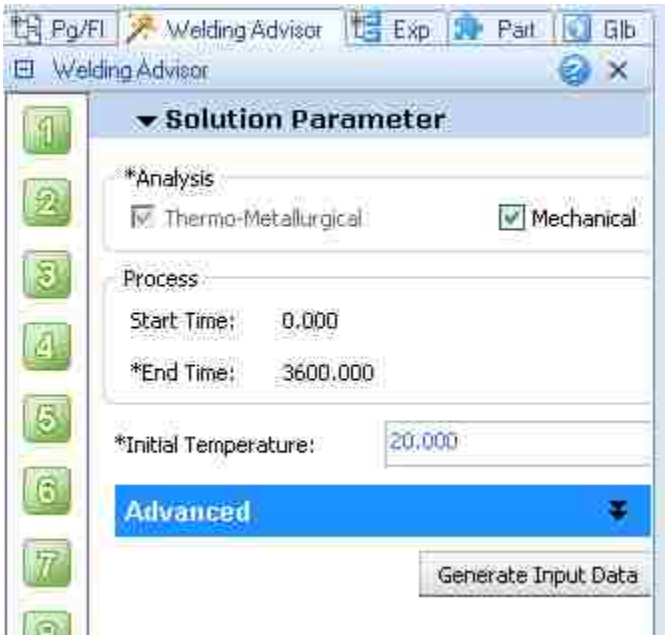

Figure 3.10 Setting up solution parameter

In the end the definition of the welding simulation has been finished, and we can simulate the welding process and get the thermo-metallurgical and mechanical results.

Chapter 4. Welding simulation results

4.1 Heat transfer behavior

The temperature contours from transient heat transfer welding simulations for 316L are shown in Figure 4.1. In this model, the welding heat source moves at a speed of 6.329 mm/s. The fitted heat source matches quite well with the melt zone which can be observed in the experiments, and it is expected that this is a reasonably good approximation for the transient temperature distribution during welding. Figure 4.1(c) shows the max shape of the temperature contour at time t =3.160s. At time t=3.160s, the temperatures of the material in the welding zone are all greater than 1400℃, which represents complete melting of 316L austenitic stainless steel in the welding zone.

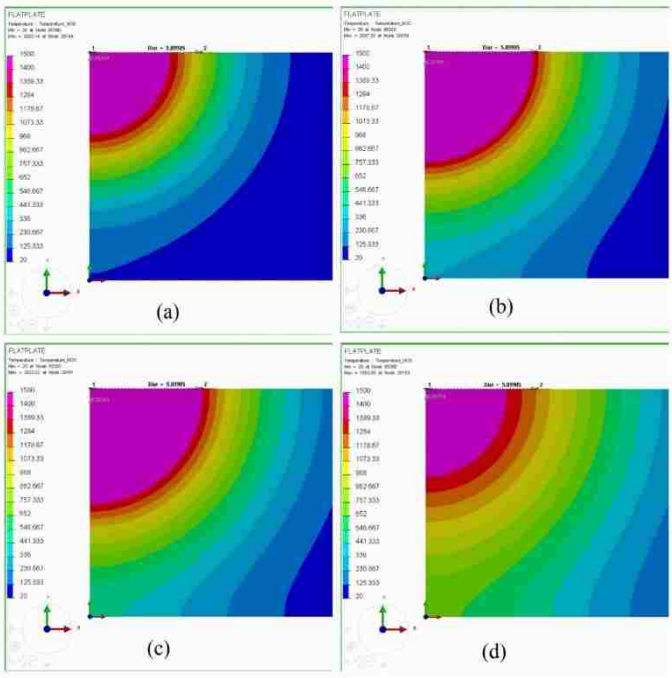

Figure 4.1 Temperature contours of 316L: (a) t=1.264s, (b) t=2.528s, (c) t=3.160s, and (d) t=5.000s.

The temperatures of nodes on the top surface of the flat plate at different times for 316L are shown in Figure 4.2. This figure depicts the transient temperature distribution immediately after the weld is deposited and the subsequent surface cooling during the first five seconds. The black horizontal line in Figure 4.2 denotes 1400℃, and the blue curve in Figure 4.2 shows the temperatures of the nodes on the top surface of the flat plate at time =3.160s. As shown by this curve, the maximum extent of the melted zone on the plane surface occurs at time t=3.160s. This position is located at x=5.92mm on the top surface of the flat plate.

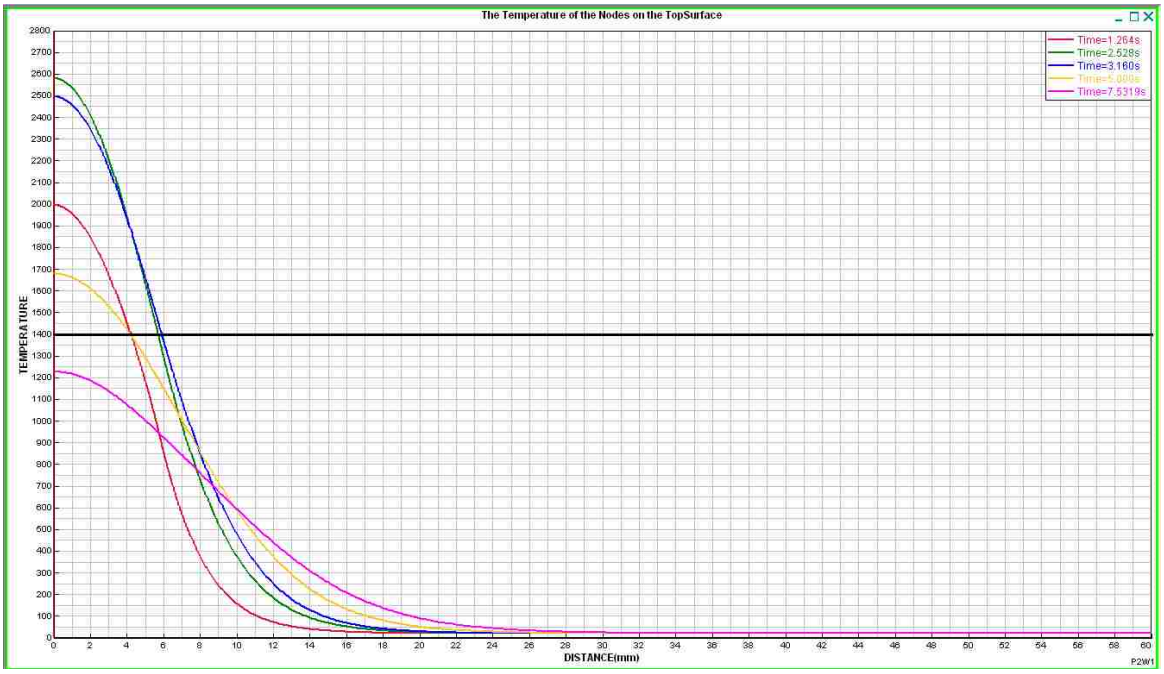

Figure 4.2 Distributions of temperature on top surface of flat plate for 316L

Figure 4.3 shows the temperature contours from the transient heat transfer welding simulations for S355J2G3. The velocity of the welding heat source is the same as used for 316L, i.e., a speed of 6.329 mm/s. The maximum edge of the melt temperature contour is shown in Figure 4.3(c), which also occurs at t=3.160s. The temperatures of the nodes in

the welding zone are all greater than 1500℃ at time t=3.160s, thus the S355J2G3 carbon steel has completely melted in the welding zone.

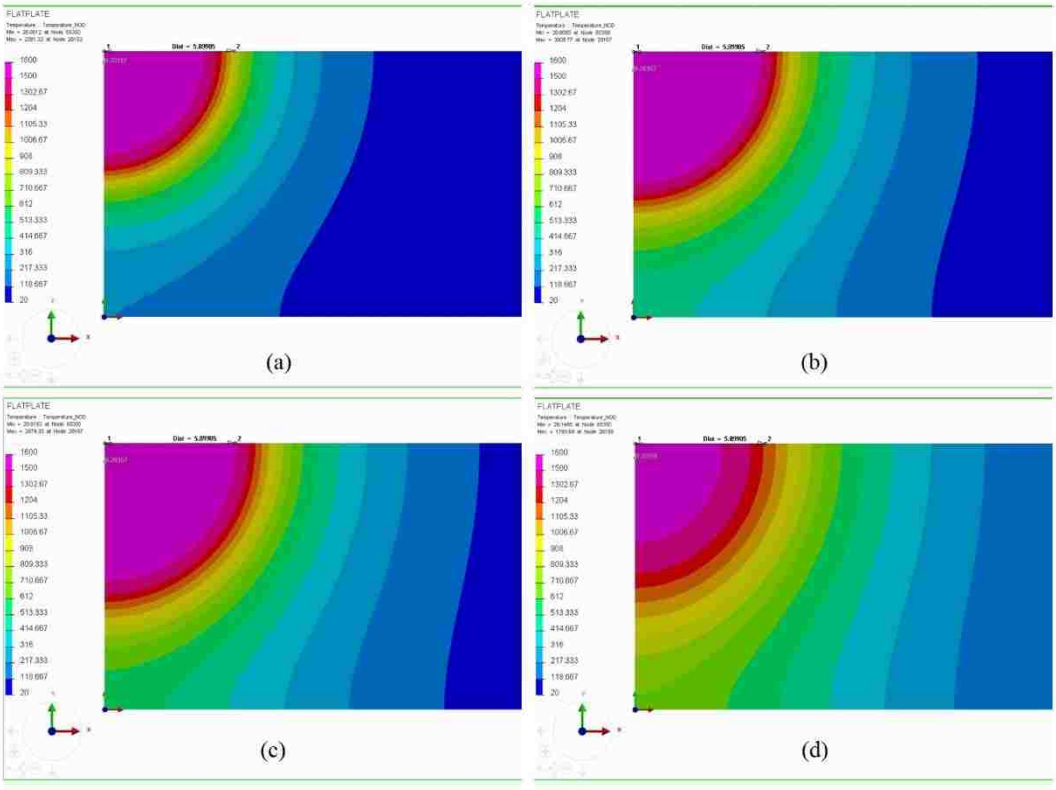

Figure 4.3 Temperature contours of S355J2G3: (a) t=1.264s, (b) t=2.528s, (c) t=3.160s, and (d) t=5.000s.

Figure 4.4 shows the temperature of the nodes on the top surface of the flat plate at the different times for S355J2G3. It depicts the transient temperature distribution immediately after the weld is deposited and the subsequent surface cooling during the first five seconds. The intersection between the horizontal line of 1500℃ (black line) and the blue curve in Figure 4.4 shows the furthermost extent of the melt pool on the top surface of the flat plate at time t=3.160s. For S355J2G3 carbon steel, the melting temperature boundary is located at x=5.94mm on the top surface of the flat. It can be seen that the

energy inputs for the two different materials have been intestinally adjusted so that there is only a small difference (0.02mm) in the extent of the melt zone between the two different materials, 316L and S355J2G3.

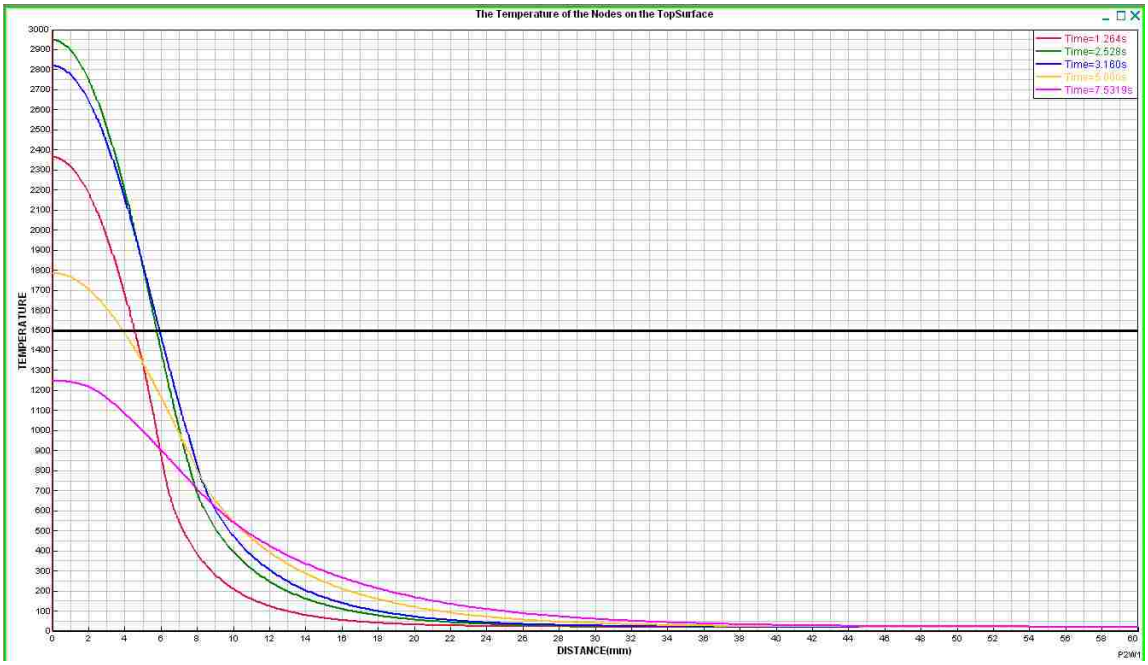

Figure 4.4 Distributions of temperature on top surface of flat plate for S355J2G3

4.2 Mechanical results for the 316L austenitic stainless Steel

The results for boundary condition 2, where the structure is clamped along the horizontal bottom-plane during welding, with properties for 316L austenitic stainless steel, will be given first. The results obtained from boundary condition 2, will be compared with the results obtained from welding simulations with boundary condition 1, i.e., no clamping restraints.

Because 316L austenitic stainless steel does not involve the additional complication of phase changes and transformation plasticity [4], the results obtained using 316L austenitic stainless steel material properties will serve as a baseline for comparison with the results from S355J2G3 carbon steel. Figure 4.5 shows the σ_{xx} stress component at two different times during the welding process. Figure 4.5(a) depicts the σ_{xx} stress in the intensely heated material immediately after the weld has been made (t=5s), with the majority of the metal plate still at ambient temperature. As shown in Figure 4.5(b), after the welded metal solidifies and has partially cooled (t=600s), there are now high tensile residual stresses, especially on the plate's top surface.

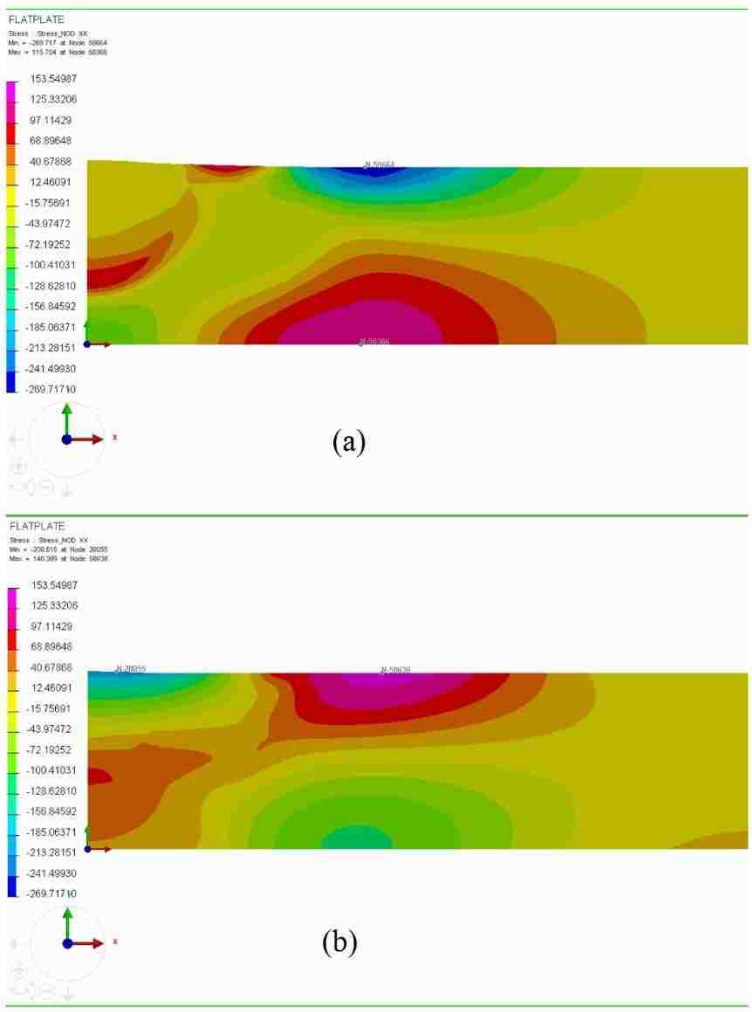

Figure 4.5 σ_{xx} stress component at two different times for 316L. (a) t=5s, (b) t=600s.

The σ_{xx} residual stresses shown in Figure 4.6(a), are the residual stresses after the structure has cooled down to the room temperature at time t=3600s. After time t=3600s, the boundary condition 2, the clamped boundary condition, is changed to a traction free boundary, boundary condition 3, i.e., the unclamped boundary condition. A slight spring back of the horizontal flat plate in the positive y-direction, vertically upwards, is results from the unclamping condition (Figure 4.7). A comparison of the σ_{xx} residual stresses before and after release of the clamped boundary conditions is shown in Figure 4.6. As shown in Figure 4.6, unclamping causes a critical change in the final residual stresses,

especially noticeable on the top surface of the flat plate. The evolution of the final residual stresses is quite complex, even in the absence of phase change related stresses.

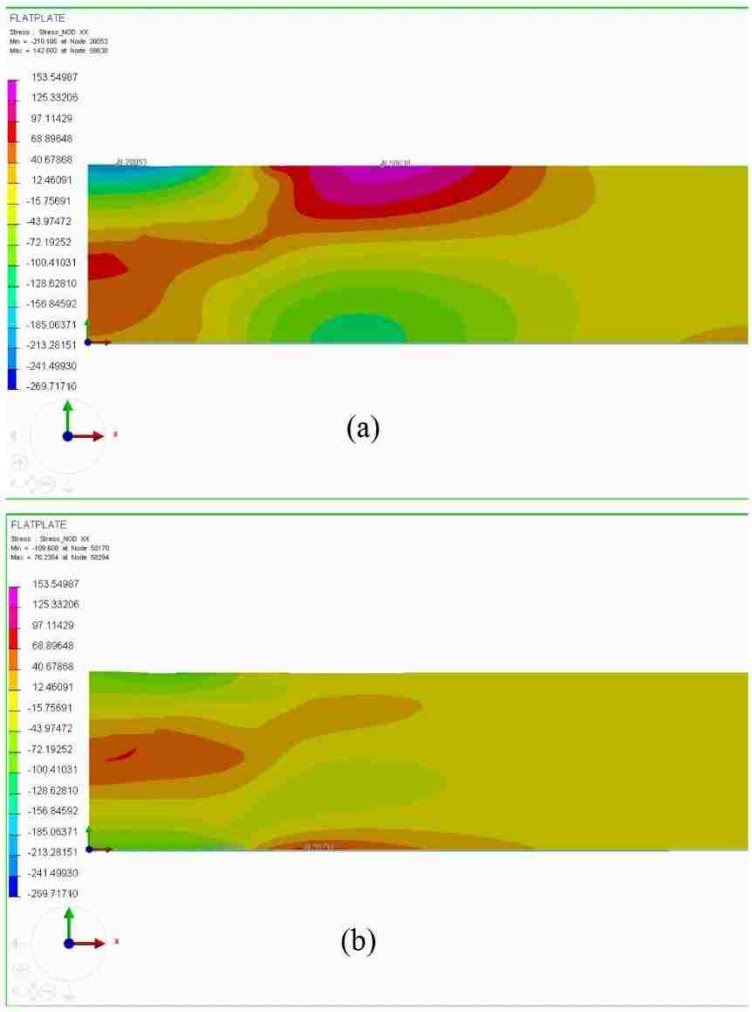

Figure 4.6 σ_{xx} stress component at two different times for 316L. (a) t=3600s, (b) t=3601s (all clamping restraints removed).

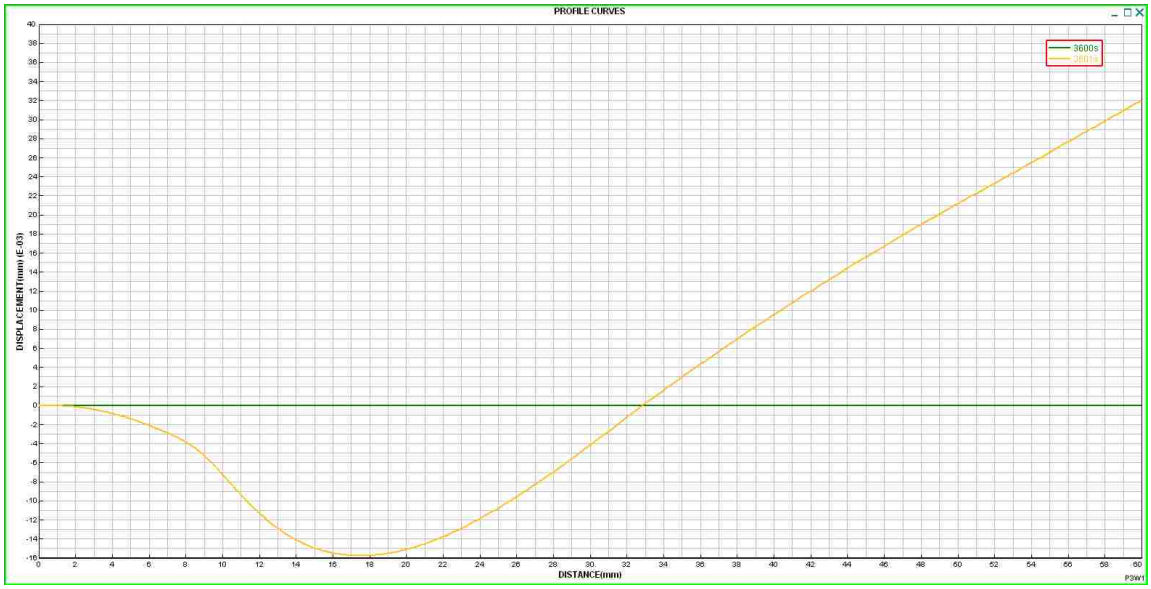

Figure 4.7 Distributions of displacement on bottom-plane for 316L

The plots shown in Figure 4.8 can be used to better understand how the residual stresses on the top surface of the flat plate evolve during the entire welding simulation. Figure 4.8 shows the σ_{xx} stress component on the top surface of the flat plate. The black vertical line is the melting boundary line where the temperature is 1400℃ and x=5.92mm. The green curve depicts the σ_{xx} stress component on the top surface of the flat plate after the weld has been deposited and the entire structures has cooled down to the room temperature, yet still while the clamping conditions are maintained. The maximum compressive surface residual stresses occurs in the melted zone close to the plane of symmetry and has a magnitude of σ_{xx}=-210 MPa. Immediately beyond the melting line, the maximum residual stress is still compressive with a value of about -185.149 MPa. This compressive stress is located at x≈5.921mm on the surface of the plate. The maximum tensile residual stress is about 142.602MPa, occurring at x≈19.994mm. The blue curve in Figure 4.8 shows the final residual stresses on the top surface of the flat plate after the clamping constraints have been released. There is a dramatic change in the magnitude and

sign of the residual stresses after release of the clamped boundary. The maximum compressive stress on the surface is σ_{xx}=-104.435MPa, occurring at x≈5.924mm, and the maximum tensile residual stress is about 16.693MPa at x≈13.066mm.

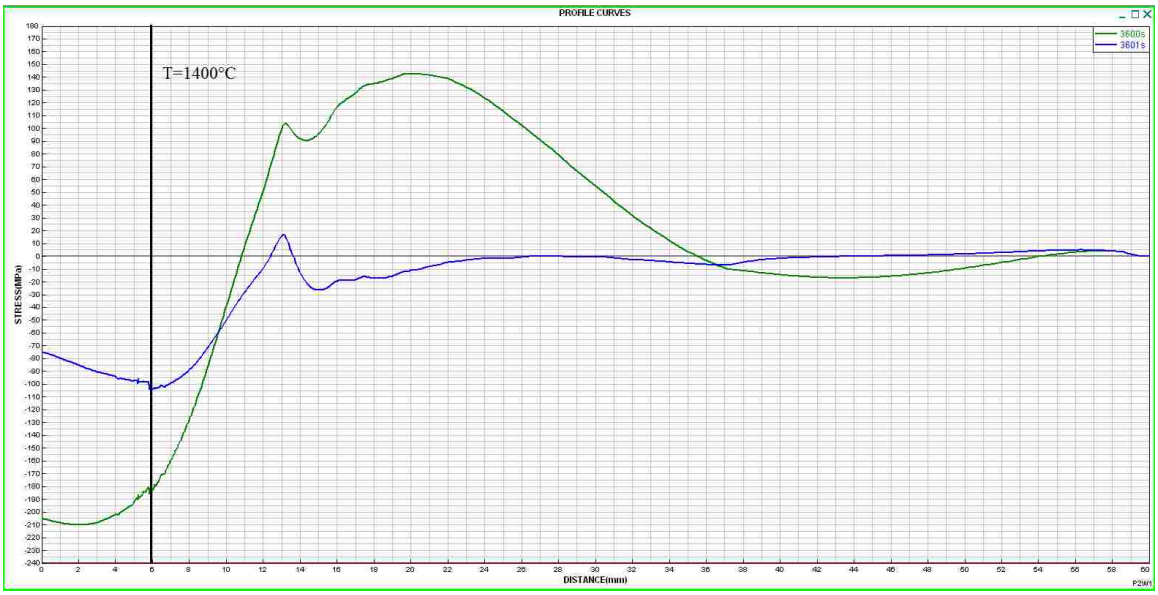

Figure 4.8 Distribution of residual stresses on top surface for 316L

In order to better understand the distribution of the residual stresses on a circular arc that approximately delineates the welding zone (green curve shown in Figure 4.9), the σ_{xx}, σ_{yy}, and σ_{xy} stress components are used to calculate the σ_{rr} and $\sigma_{\theta\theta}$ stress components.

$$\sigma_{rr} = \sigma_{xx}cos^2\theta + 2\sigma_{xy}sin\theta cos\theta + \sigma_{yy}sin^2\theta \ldots\ldots (4.1)$$

$$\sigma_{\theta\theta} = \sigma_{xx}sin^2\theta - 2\sigma_{xy}sin\theta cos\theta + \sigma_{yy}cos^2\theta \ldots\ldots (4.2)$$

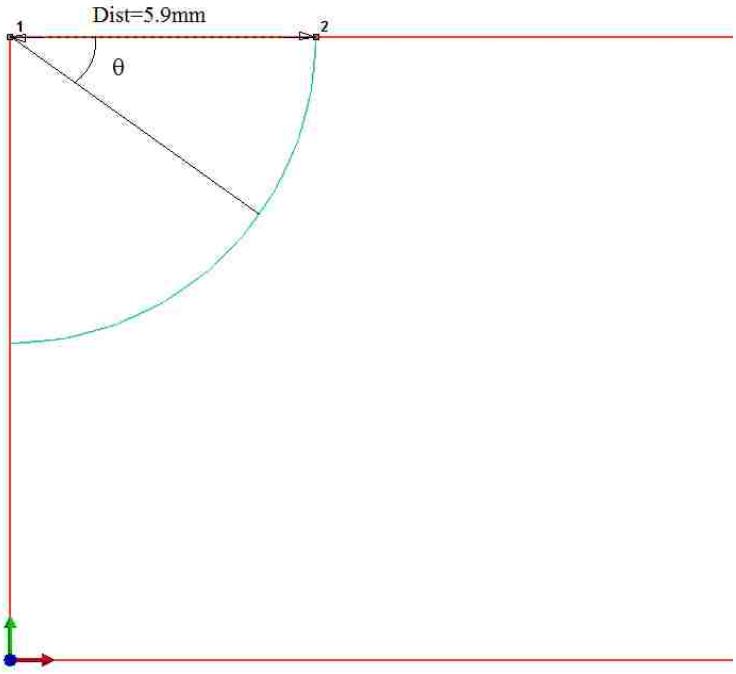

Figure 4.9 Position of maximum radius of welding zone

Figure 4.10 shows the σ_{rr} and $\sigma_{\theta\theta}$ stress components during clamping and after unclamping. In Figure 4.10(a), the blue curve represents the σ_{rr} stress component at time t=3600s with clamped boundary conditions. The maximum absolute value of σ_{rr} is located at $\theta \approx 1.0624°$, and its value is about σ_{rr}=-181.025MPa. In Figure 4.10(b), the blue curve depicts the σ_{rr} stress component at time t=3601s, i.e., after unclamping. In this case, the maximum absolute value of σ_{rr} happens at $\theta \approx 1.0864°$, and its value is about σ_{rr}=-99.889MPa. Figure 4.10(c) and Figure 4.10(d) provide a comparison of the final residual stress state on the max radius of the welding zone for 316L austenitic stainless steel. As can be seen in these plots, the changing trends of the residual stresses before and after release of the clamped boundary conditions are very similar. In Figure 4.10(c), the residual stresses both rise in the beginning then decline slightly.

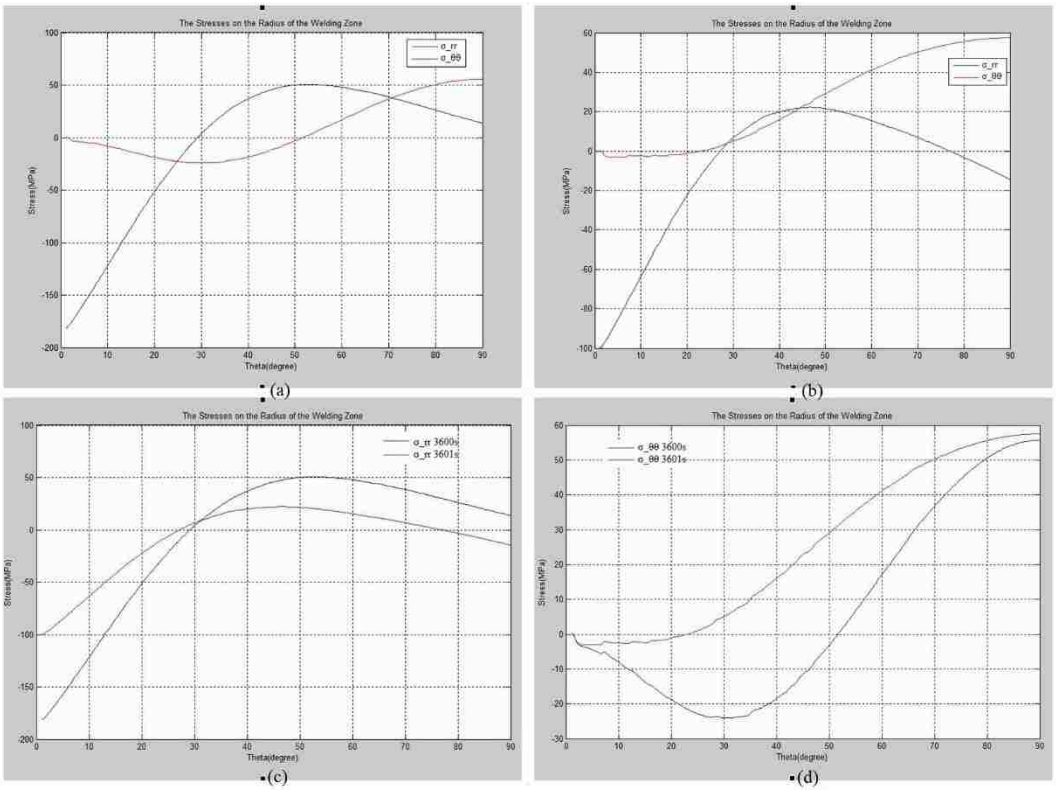

Figure 4.10 Distributions of the σ_{rr} and $\sigma_{\theta\theta}$ stress components along maximum radius of welding zone for 316L. (a) boundary condition 2, (b) boundary condition 3, (c) comparison of σ_{rr}, (d) comparison of $\sigma_{\theta\theta}$.

The mechanical results with the boundary condition 2 and 3 indicate that the residual stress state for 316L austenitic stainless steel are seriously influenced by the boundary conditions. In an attempt to determine how the residual stresses will change with different boundary conditions, the results obtained from the welding simulation under the boundary condition 1, with no clamping restraints on the bottom-plane during the entire welding process, are compared with the previous results.

Figure 4.11 shows the comparison between the residual stresses on the top surface of the flat plate for 316L austenitic stainless steel for the different boundary conditions. The

residual stress under boundary condition 2, the green curve, is totally different than the others, the red and blue curve. The clamped boundary condition appears to result in larger residual stresses than would occur when welding an unclamped plate. But the changing trends of the residual stresses under the boundary condition 1 and 3 are a little similar. Figure 4.12 shows the comparison between the residual stresses on the maximum radius of the welding zone of the flat plate for 316L austenitic stainless steel in different boundary conditions. There is a little difference in the residual stress component, σ_{rr}, between the unclamped boundary condition during the entire welding process (green curve) and after release of the clamped boundary condition (red curve).

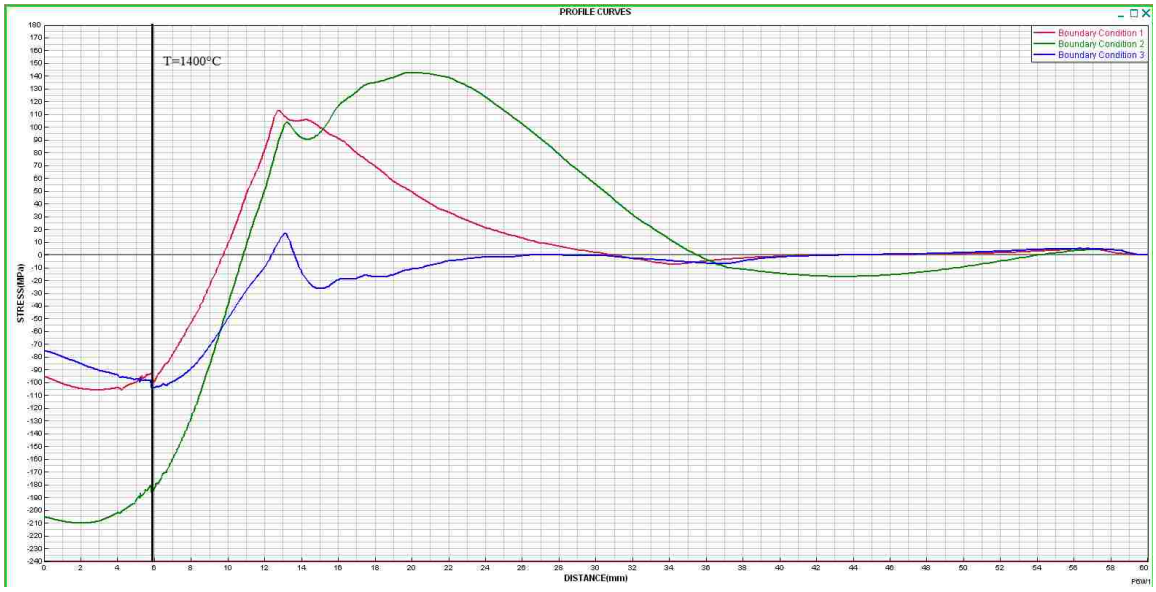

Figure 4.11 Comparison of residual stresses on top surface for 316L under different boundary conditions

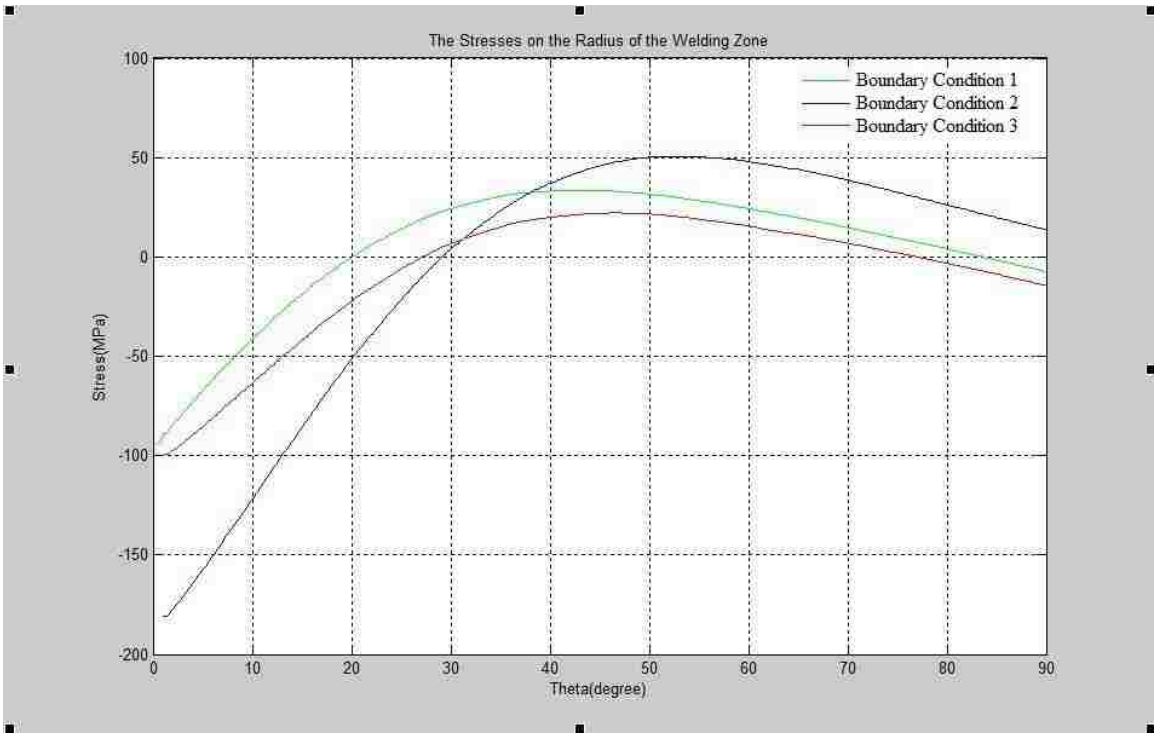

Figure 4.12 Comparison of residual stresses on maximum radius of welding zone for 316L under different boundary conditions

4.3 Mechanical results for the S355 carbon steel

The discussion of the results for S355J2G3 carbon steel is similar with 316L's. With the boundary condition 2, the structure clamped along the horizontal bottom-plane during welding, the residual stresses acquired using the properties of the material, S355J2G3 carbon steel, will be represented first. The results obtained from the boundary condition 2, the clamped condition, will be compared with the result obtained from welding simulation with the boundary condition 1, no clamping restraints.

Figure 4.13 shows the σ_{xx} stress component at two different times during the welding process. Figure 4.13(a) shows that the intensely heated material underneath the weld attempts to spread out, but the ambient majority of the metal restrains it. The contour of the σ_{xx} stresses at time =600s is shown in Figure 4.13(b).

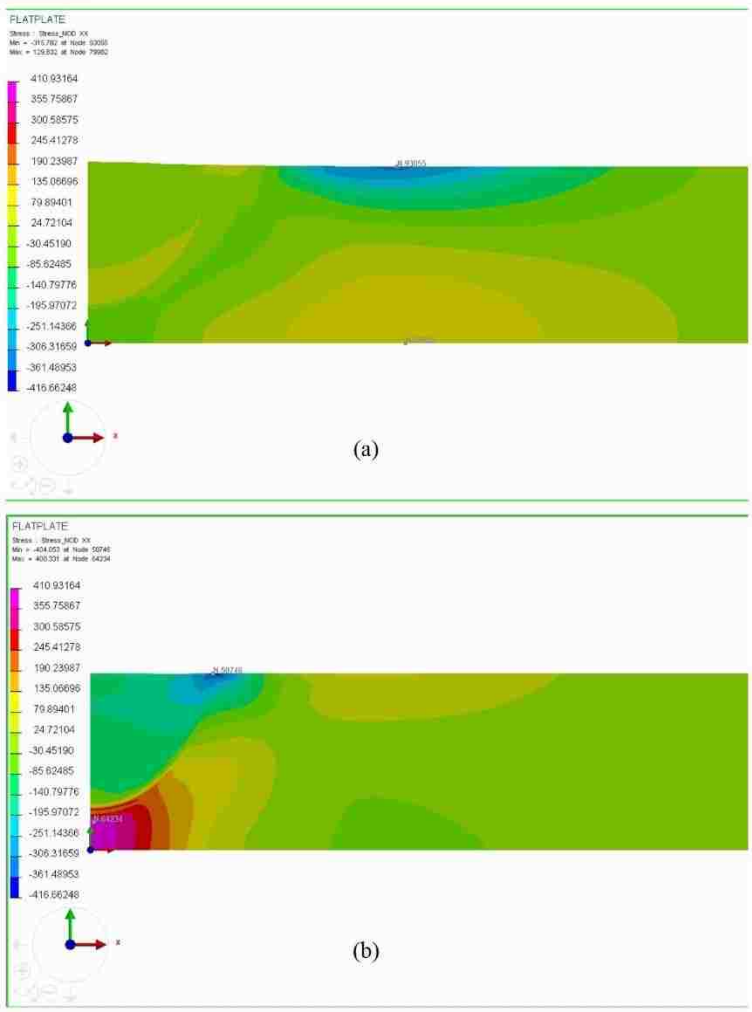

Figure 4.13 σ_{xx} stress component at two different times for S355J2G3. (a) t=5s, (b) t=600s.

The σ_{xx} residual stresses shown in Figure 4.14(a), are the residual stresses when the structure has cooled down to the room temperature at time=3600s. After time=3600s, the boundary condition 2, the clamped boundary condition, is changed to the traction free boundaries, which is the boundary condition 3, the unclamped boundary condition. A slight spring back of the horizontal flat plate in the negative y-direction, vertically downwards, is cause by the unclamped boundary condition (Figure 4.15). A comparison of the σ_{xx} residual stresses before and after release of the clamped boundary conditions is shown in

Figure 4.14. As shown in Figure 4.14, unclamping can cause a critical important change in the final residual stresses for S355J2G3 carbon steel.

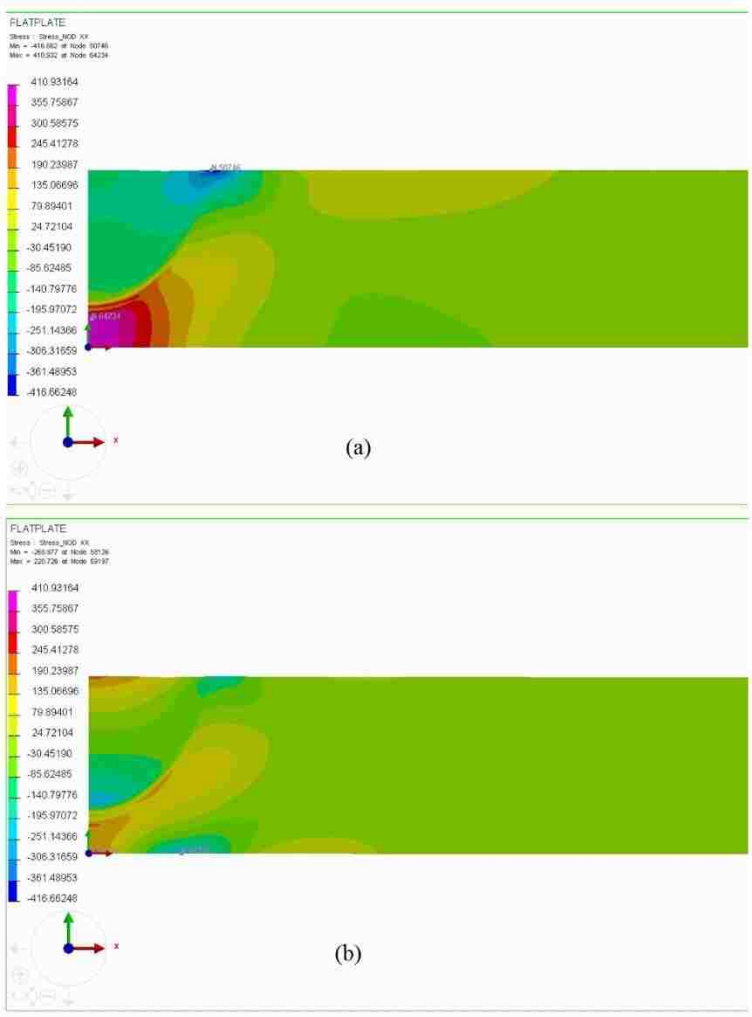

Figure 4.14 σ_{xx} stress component at two different times for S355J2G3. (a) t=3600s, (b) t=3601s.

Figure 4.15 Distributions of displacement on bottom-plane for S355J2G3

Comparisons with the equivalent figures for 316L austenitic stainless steel show that the spatial distributions of the residual stresses are quite different. Figure 4.16 shows the σ_{xx} stress component on the top surface of the flat plate for S355J2G3 carbon steel. The black straight line is the melting line where the temperature is 1500℃, and x=5.94mm. The red curve depicts the σ_{xx} stress component on the top surface of the flat plate after the weld has been deposited and the entire structures has cooled down to the room temperature, yet still while the clamping conditions are maintained. As can be seen, after the melting line the maximum absolute value of the residual stress, which value is about -416.662MPa, happens at x≈8.343mm. Finally, the green curve shows the final residual stresses on the top surface of the flat plate after clamping constraints are released. Based on the green curve, after melting line the maximum absolute value of the residual stress, which value is about -231.822MPa, happens at x≅8.453mm.

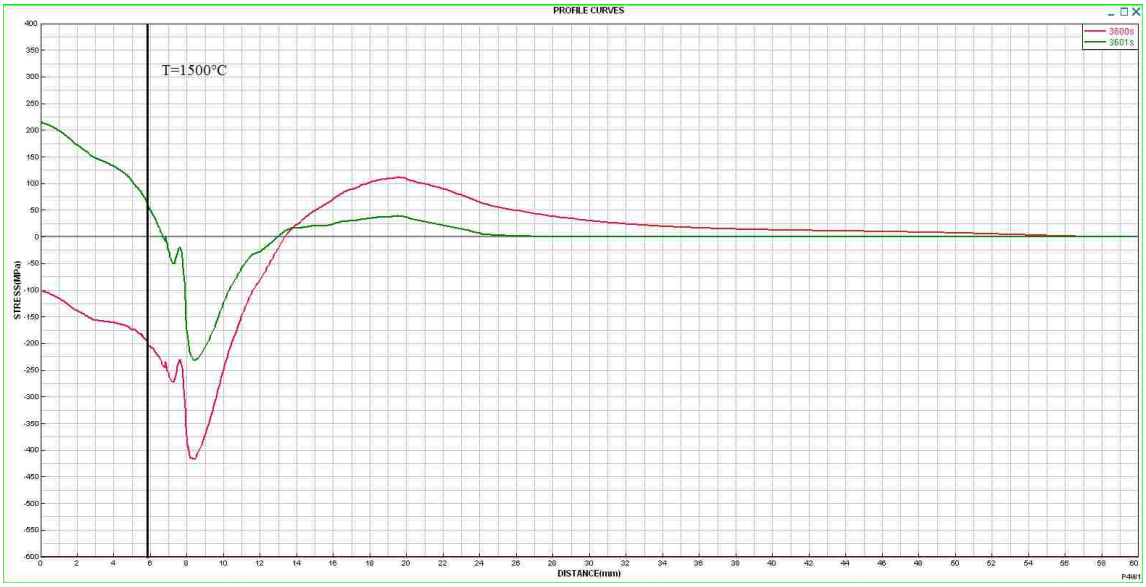

Figure 4.16 Distribution of residual stresses on top surface for S355J2G3

In order to understand the distribution of the residual stresses on the max radius of the welding zone (the highlight green curves shown in Figure 4.9), the σ_{xx}, σ_{yy}, and σ_{xy} stress components should be changed to σ_{rr} and $\sigma_{\theta\theta}$.

Figure 4.17 shows that how the σ_{rr} and $\sigma_{\theta\theta}$ stress components for S355J2G3 carbon steel evolve during clamping and unclamping during the entire welding simulation. In Figure 4.17(a), the blue curve stands for the σ_{rr} stress component at time =3600s with the clamped boundary conditions. The maximum absolute value of σ_{rr} happens at $\theta \approx 9.9438°$, and its value is about -219.145MPa. In Figure 4.17(b), the blue curve is the σ_{rr} stress component at time =3601s with the unclamped boundary conditions. The maximum absolute value of σ_{rr} happens at $\theta \approx 46.8561°$, and its value is about -153.089MPa. Figure 4.17(c) and Figure 4.17(d) provide a comparison of the final residual stress state on the max radius of the welding zone for S355J2G3 carbon steel. As can be seen in these plots,

the changing trends of the residual stresses before and after release of the clamped boundary conditions are very different.

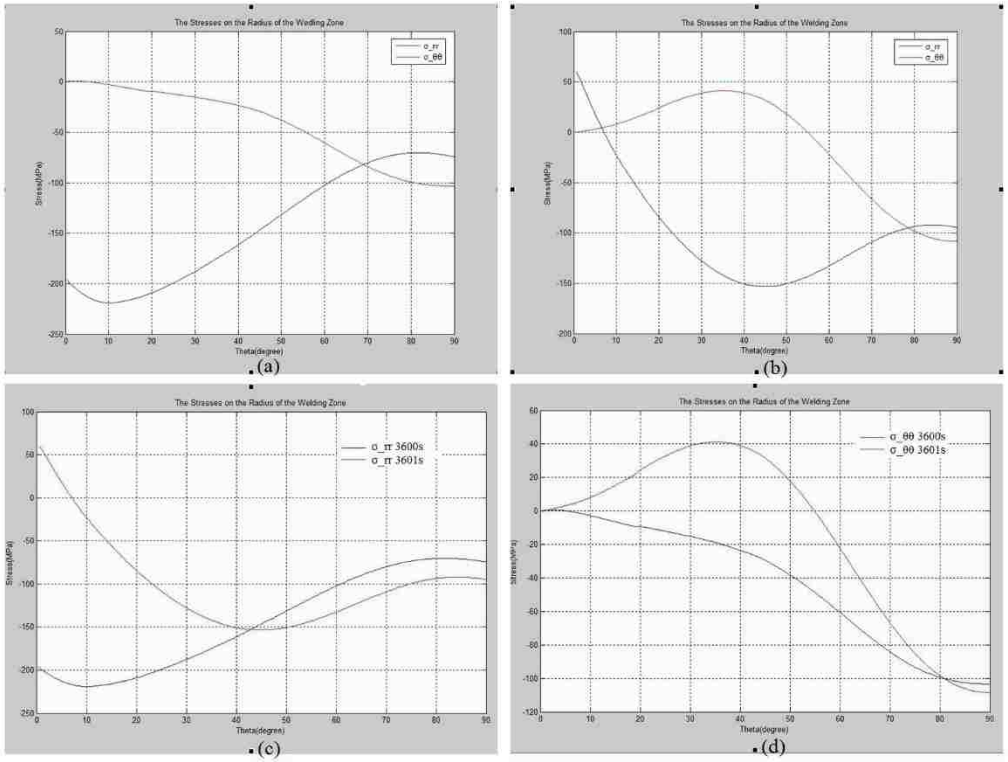

Figure 4.17 Distributions of the σ_{rr} and $\sigma_{\theta\theta}$ stress components along maximum radius of welding zone for S355J2G3. (a) boundary condition 2, (b) boundary condition 3, (c) comparison of σ_{rr}, (d) comparison of $\sigma_{\theta\theta}$.

According to the analysis of the above mechanical results, it concludes that the residual stress state for S355J2G3 carbon steel are critical influenced by the boundary conditions. In an attempt to determine how the residual stresses will change with the different boundary conditions, the results obtained from the welding simulation under the boundary condition 1, no clamping restraints on the bottom-plane during the entire welding process, is made to be a comparison.

Figure 4.18 shows the comparison between the residual stresses on the top surface of the flat plate for S355J2G3 carbon steel in different boundary conditions. The residual stress under the boundary condition 2, the green curve, is totally different with the others, the red and blue curve, and the clamped boundary condition will produce much bigger residual stresses than others. But the changing trends of the residual stresses under the boundary condition 1 and 3 are very close.

Figure 4.19 shows the comparison between the residual stresses on the maximum radius of the welding zone of the flat plate for S355J2G3 carbon steel in different boundary conditions. There is a little difference of residual stress, σ_{rr}, between the unclamped boundary condition during the entire welding process (blue curve) and after release of the clamped boundary condition (red curve).

Figure 4.18 Comparison of residual stresses on top surface for S355J2G3 under different boundary conditions

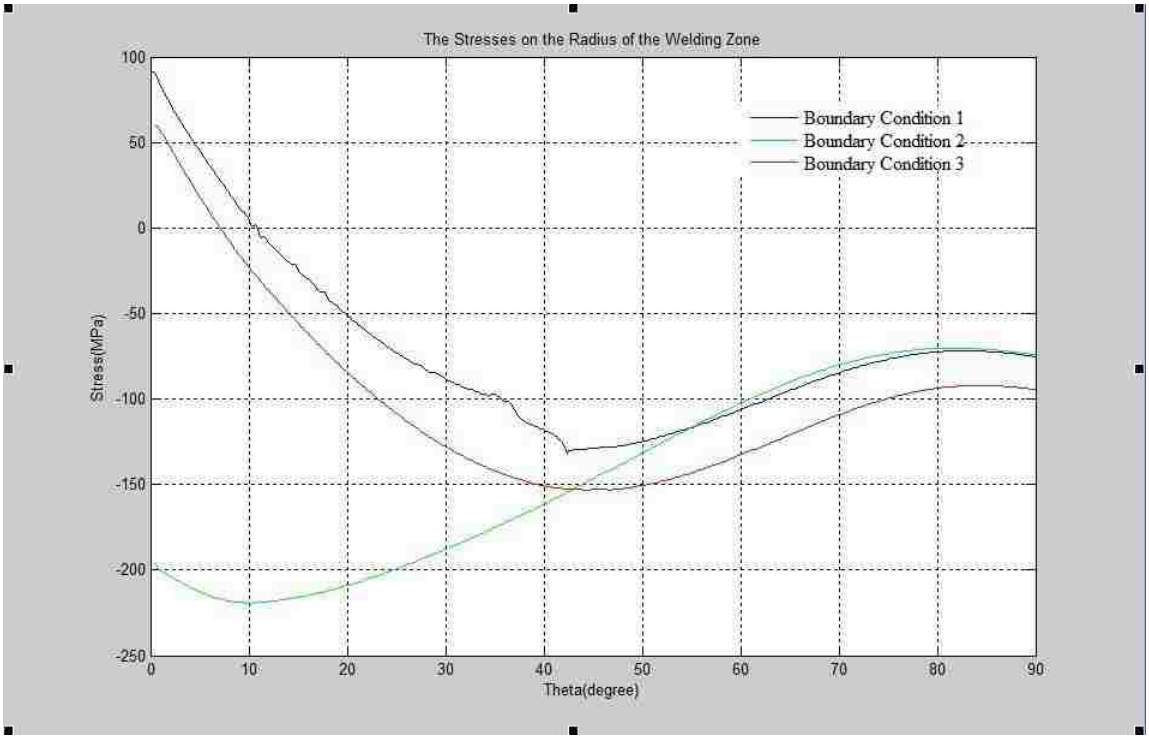

Figure 4.19 Comparison of residual stresses on maximum radius of welding zone for S355J2G3 under different boundary conditions

Figure 4.20 provides a direct comparison of the residual stresses on the top surface and the max radius of the welding zone of the flat plate for 316L austenitic stainless steel and S355JG3 carbon steel. Under the boundary condition 1, the unclamped condition during the entire welding process, Figure 4.20(a) shows the comparison of the residual stresses on the top surface between 316L austenitic stainless steel and S355J2G3 carbon steel, and Figure 4.20(d) shows the comparison of the residual stresses on the max radius of the welding zone between the two materials. Under the boundary condition 2, before release of the clamped condition, the residual stresses of 316L austenitic stainless steel and S355J2G3 carbon steel on the top surface are shown in Figure 4.20(b), and the residual stresses of the two materials on the max radius of the welding zone are shown in Figure 4.20(e). Under the boundary condition 3, after release of the clamped condition, Figure

4.20(c) depicts the residual stresses of 316L austenitic stainless steel and S355J2G3 carbon steel on the top surface, and Figure 4.20(f) depicts the residual stresses of the two materials on the max radius of the welding zone. According to these figures, it is very clear that the residual stresses of S355J2G3 carbon steel on the top surface of the flat plate have a much high fluctuation than 316L's.

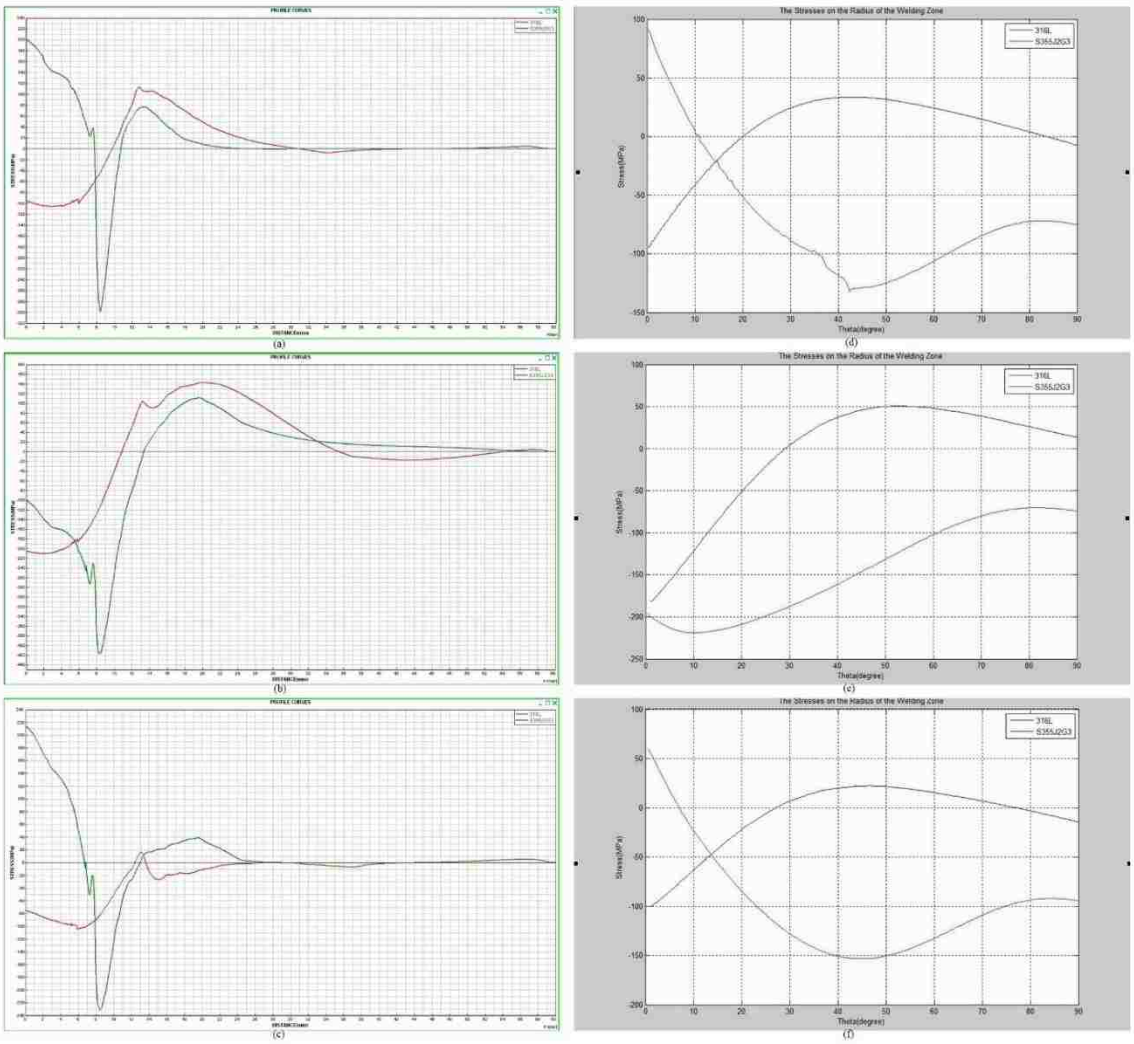

Figure 4.20 Comparison of different residual stresses for 316L and S355J2G3

4.4 Metallurgical phase in S355 carbon steel

Figure 4.21 shows the distribution of the austenite of S355J2G3 carbon steel along the top surface of the flat plate when time=5s during the welding process. Between 0 and about 7.55mm, the percentage of the austenite on the top surface is 100%, but it will decrease gradually between 7.55mm and 8.7mm. In the end there is no austenite after 8.7mm on the top surface.

Figure 4.22 shows the distribution of the ferrite of S355J2G3 carbon steel along the top surface of the flat plate after cooling. There is no ferrite between 0 and about 7.3mm on the top surface. However, the percentage of the ferrite will increase gradually between 7.3mm and 8.45mm. Finally, it will reach 100% after 8.45mm.

Figure 4.23 shows the distribution of the bainite of S355J2G3 carbon steel along the top surface of the flat plate after cooling. Between 0 and 5.5mm the percentage of the bainite will keep at 13.5%~15%, but it will decrease gradually between 5.5mm and 8.5mm. In the end there is no bainite after 8.5mm on the top surface.

Figure 4.24 shows the distribution of the martensite of S355J2G3 carbon steel along the top surface of the flat plate after cooling. The percentage of the martensite will keep at about 85% between 0 and 7.3mm, but it will decrease gradually between 7.3mm and 8.5mm. Finally there is no martensite after 8.5mm on the top surface.

Figure 4.21 Austenite distribution along top surface at 5s during welding

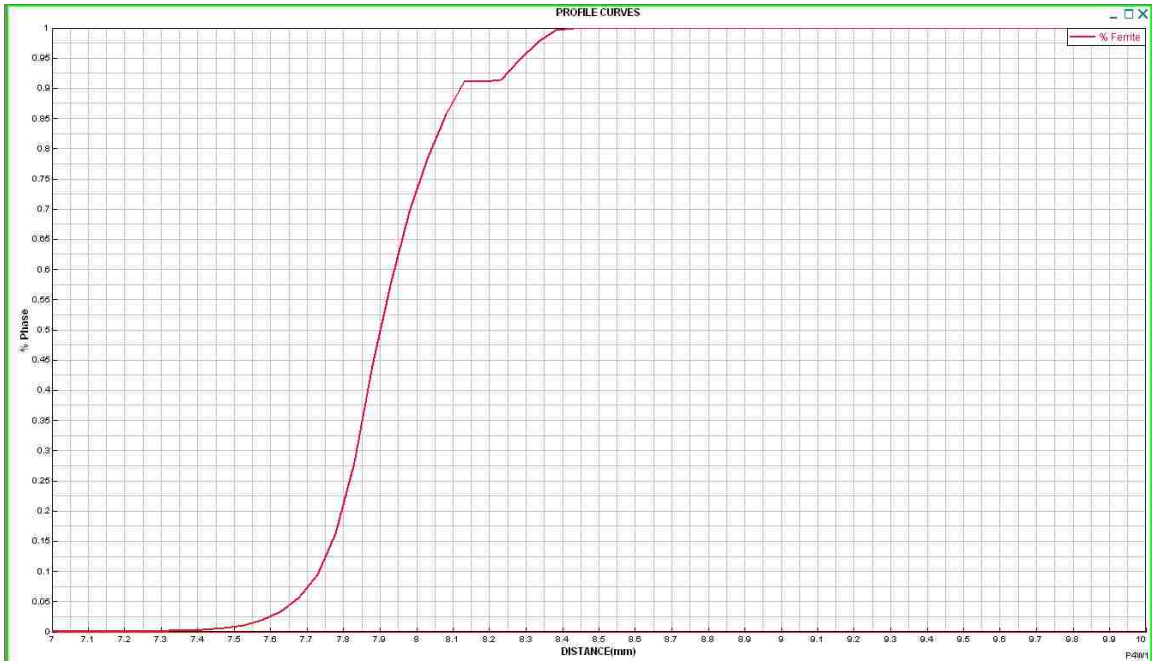

Figure 4.22 Ferrite distribution along top surface after cooling

Figure 4.23 Bainite distribution along top surface after cooling

Figure 4.24 Martensite distribution along top surface after cooling

A comparison of the distribution of the different phases is shown in Figure 4.25. As can be seen, the percentage of the austenite, ferrite, bainite, and martensite will change rapidly between 7.5mm and 8.5mm on the top surface of the flat plate.

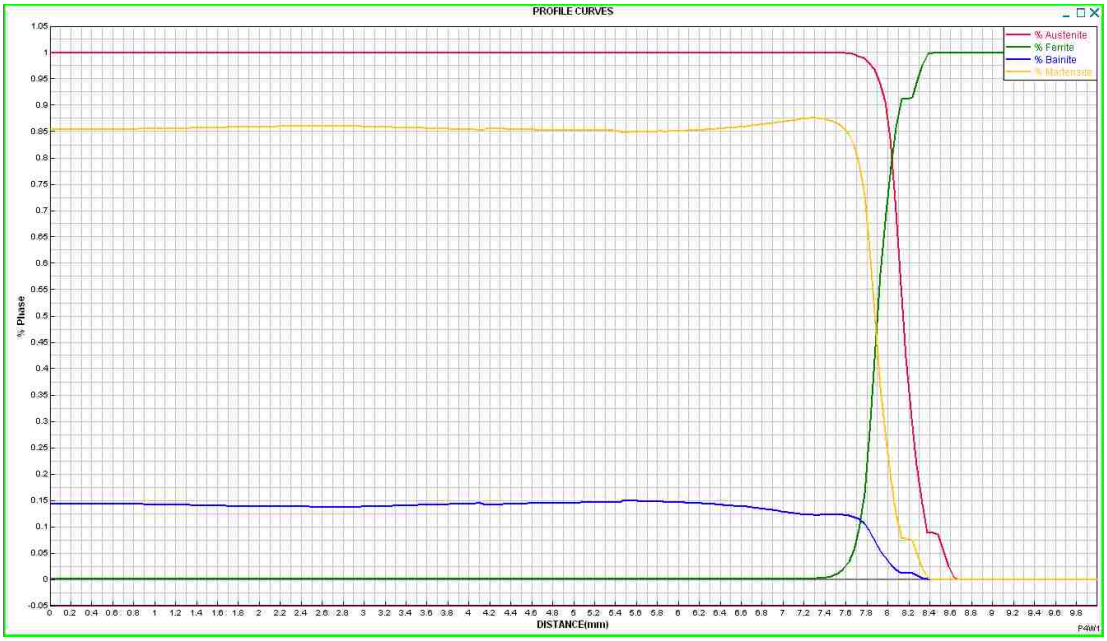

Figure 4.25 Phase distribution along top surface

4.5 Mechanical results for the S355 carbon steel without phase changes

In order to clearly understand that how the phase changes will influence the residual stresses on the top surface of the flat plate for S355J2G3 carbon steel, a welding simulation without phase changes will be made as a comparison.

Under the boundary condition 1, the unclamped condition during the entire welding process, σ_{xx} on the top surface of the flat plate (the red curve in Figure 4.26) will decrease rapidly near the melting boundary, where is about 6mm, until it reaches the negative peak value that is about -350MPa. Then σ_{xx} will rise quickly to the positive peak value that is about 260MPa. Finally σ_{xx} will decrease to zero gradually.

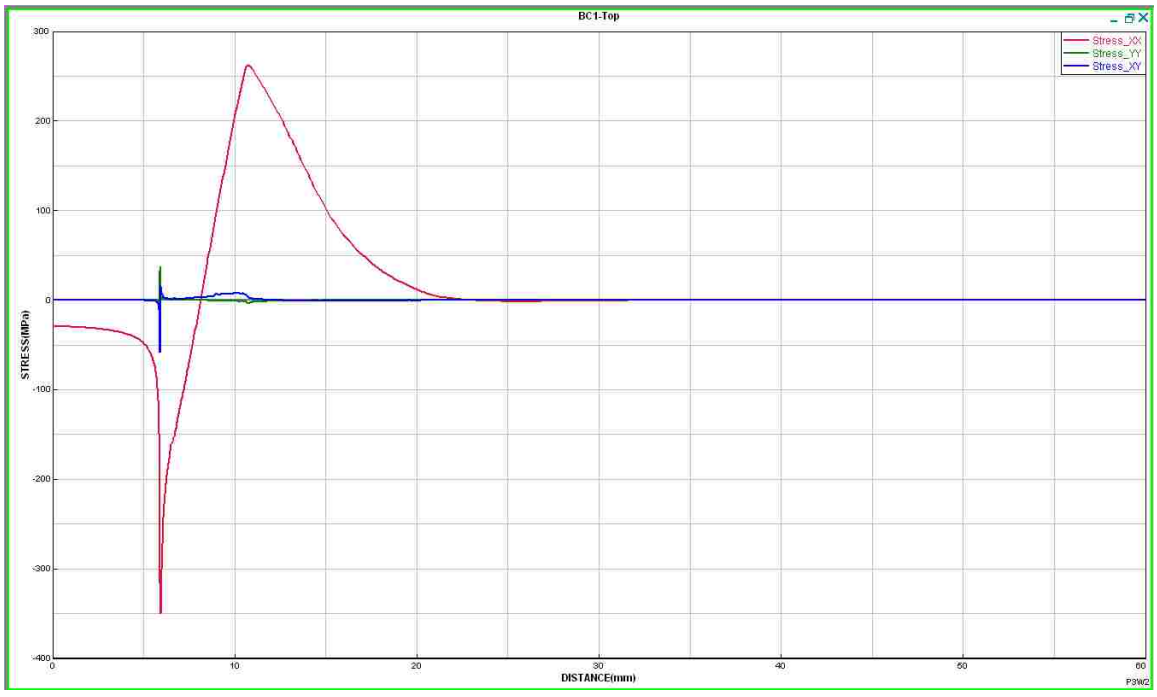

Figure 4.26 Distributions of residual stresses on top surface under boundary condition 1 for S355J2G3 without phase changes

Figure 4.27 shows σ_{xx} on the top surface of the flat plate (red curve) under the boundary condition 2, before release of the clamped condition, and Figure 4.28 depicts σ_{xx} on the top surface of the flat plate under the boundary condition 3, after release of the clamped condition. The changing trends of the red curves in Figure 4.27 and Figure 4.28 are very close to the one in Figure 46. The only differences are the peak value of σ_{xx}. For the boundary condition 2, the negative peak value of σ_{xx} is about -260MPa and the positive peak value is about 310MPa. For the boundary condition 3, the negative peak value of σ_{xx} is about -320MPa and the positive peak value is about 190MPa. Figure 4.29 clearly depicts a comparison of the distribution of the residual stresses on the top surface of flat plate for S355J2G3 without phase changes during welding process under the different boundary conditions. As can be seen, the negative peak values of σ_{xx} all happen near the melt boundary and the positive peak values of σ_{xx} always happen at about x=11mm.

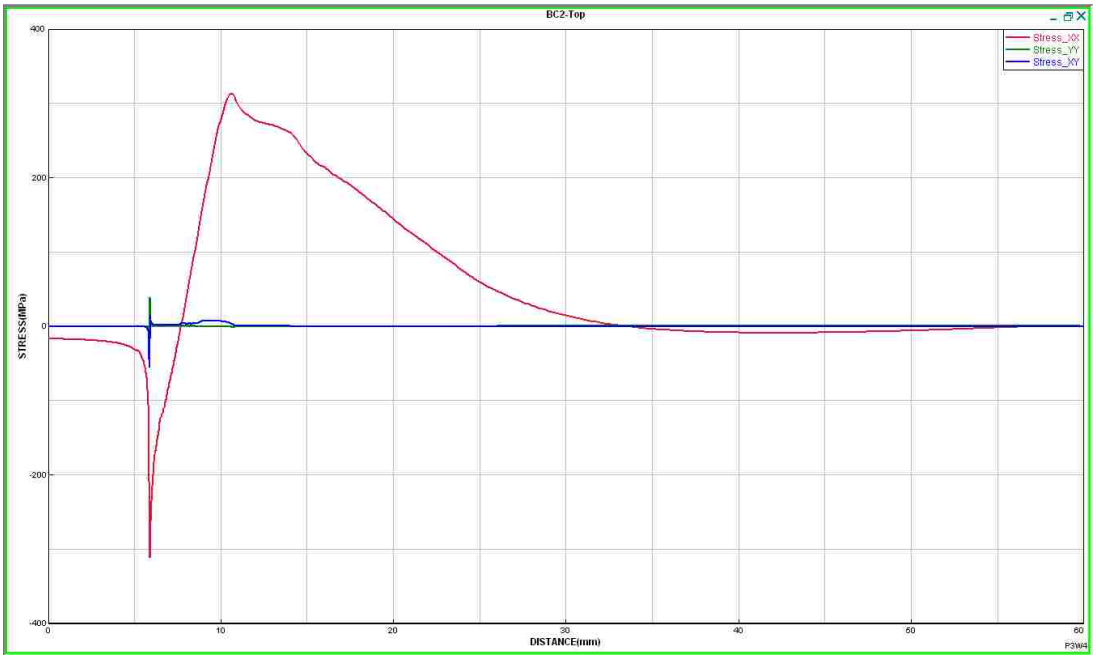

Figure 4.27 Distributions of residual stresses on top surface under boundary condition 2 for S355J2G3 without phase changes

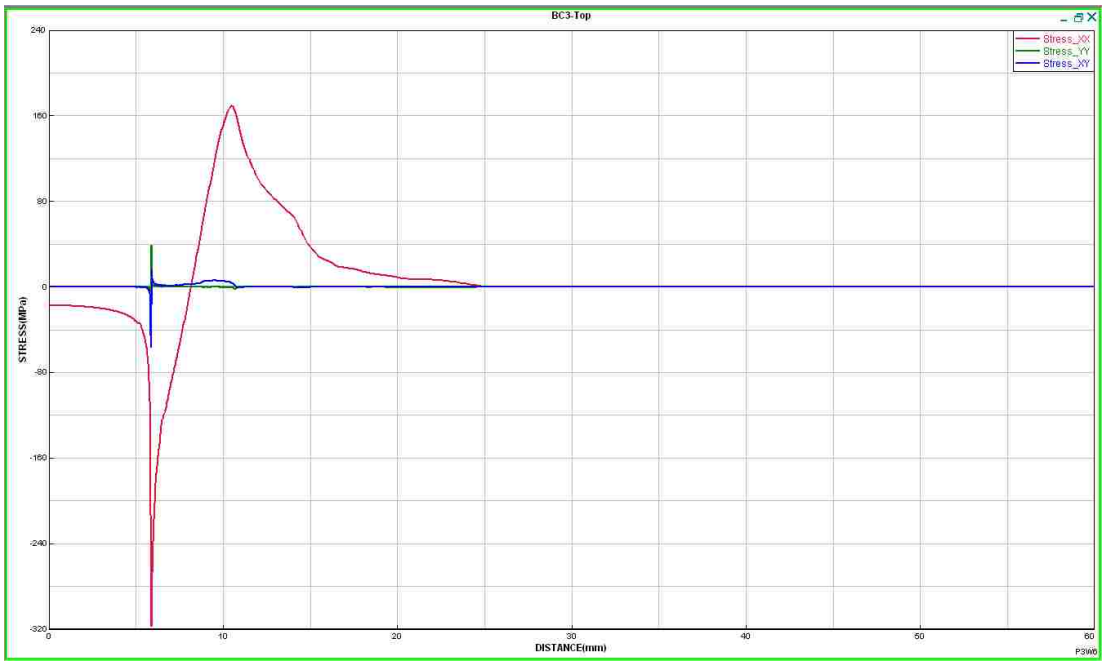

Figure 4.28 Distributions of residual stresses on top surface under boundary condition 3 for S355J2G3 without phase changes

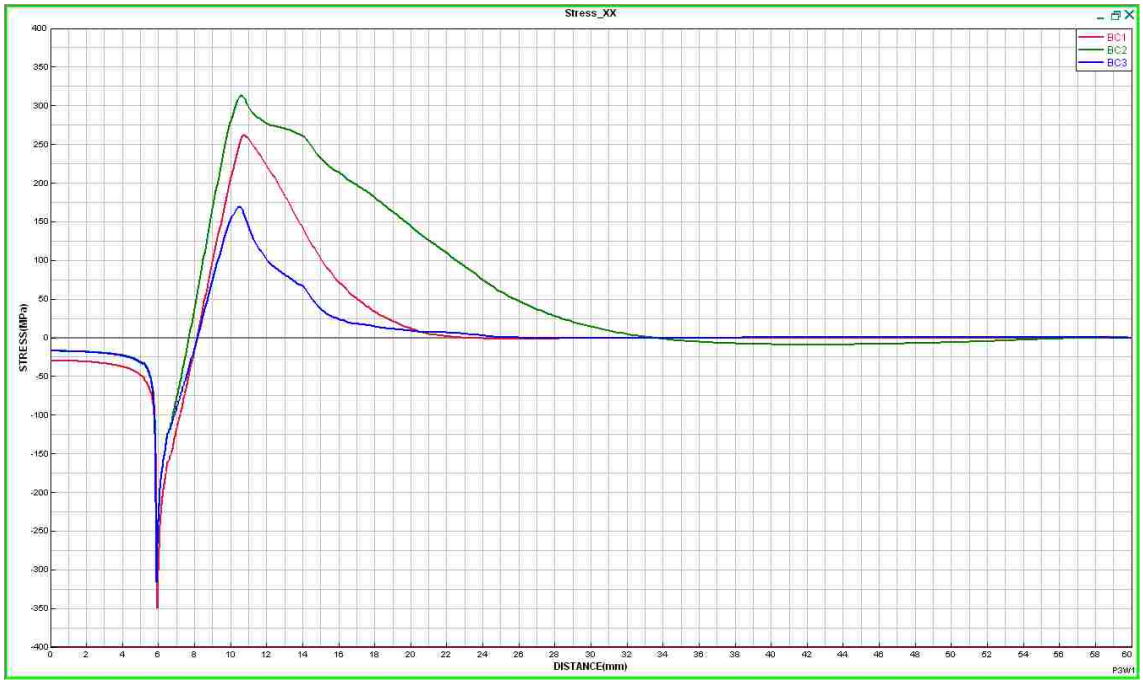

Figure 4.29 Distributions of residual stresses on top surface for S355J2G3 without phase changes

Under the boundary condition 1, the unclamped condition during the entire welding process, the residual stresses σ_{xx} on the top surface of the flat plate for 316L austenitic stainless steel, S355J2G3 carbon steel with phase changes, and S355J2G3 carbon steel without phase changes are compared in Figure 4.30. The similar comparisons of the residual stresses σ_{xx} are made in Figure 4.31 for the boundary condition 2, before release of the clamped condition, and Figure 4.32 for the boundary condition 3, after release of the clamped condition. According to the analysis of these three figures, it is clear that the residual stresses σ_{xx} on the top surface of the flat plate for S355J2G3 carbon steel without phase changes during welding process are corresponding different from the other two under every boundary condition, especially for the changing trends of them.

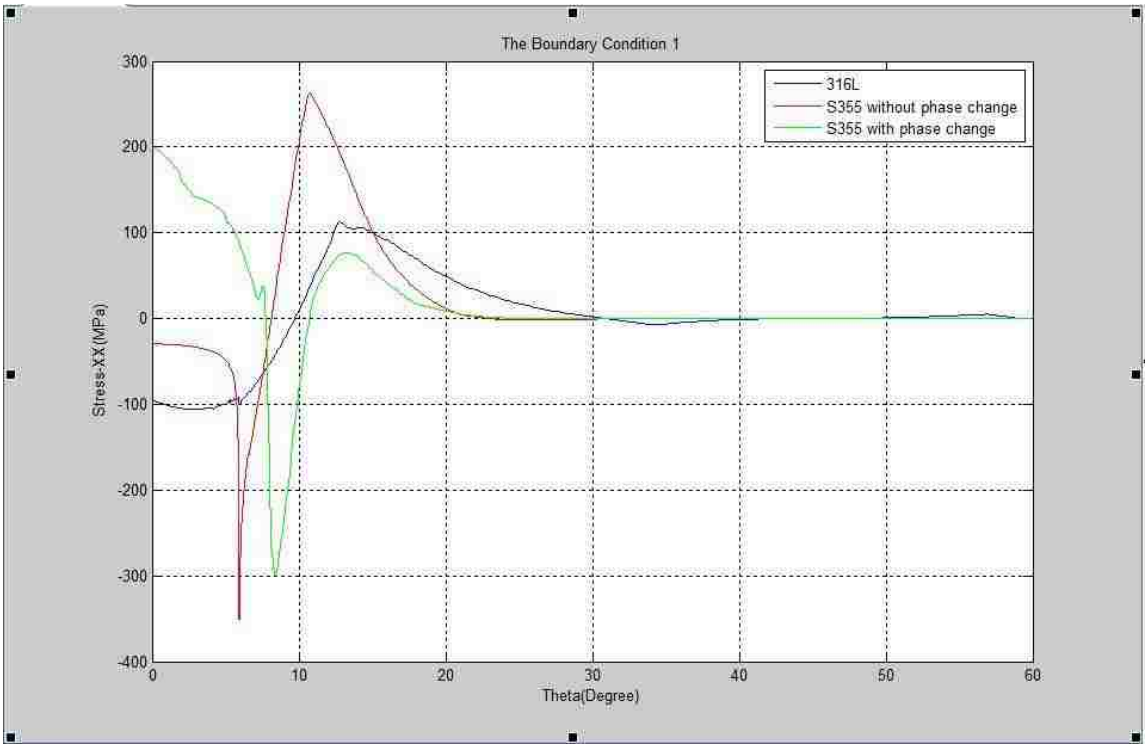

Figure 4.30 Distributions of residual stresses on top surface under boundary condition 1

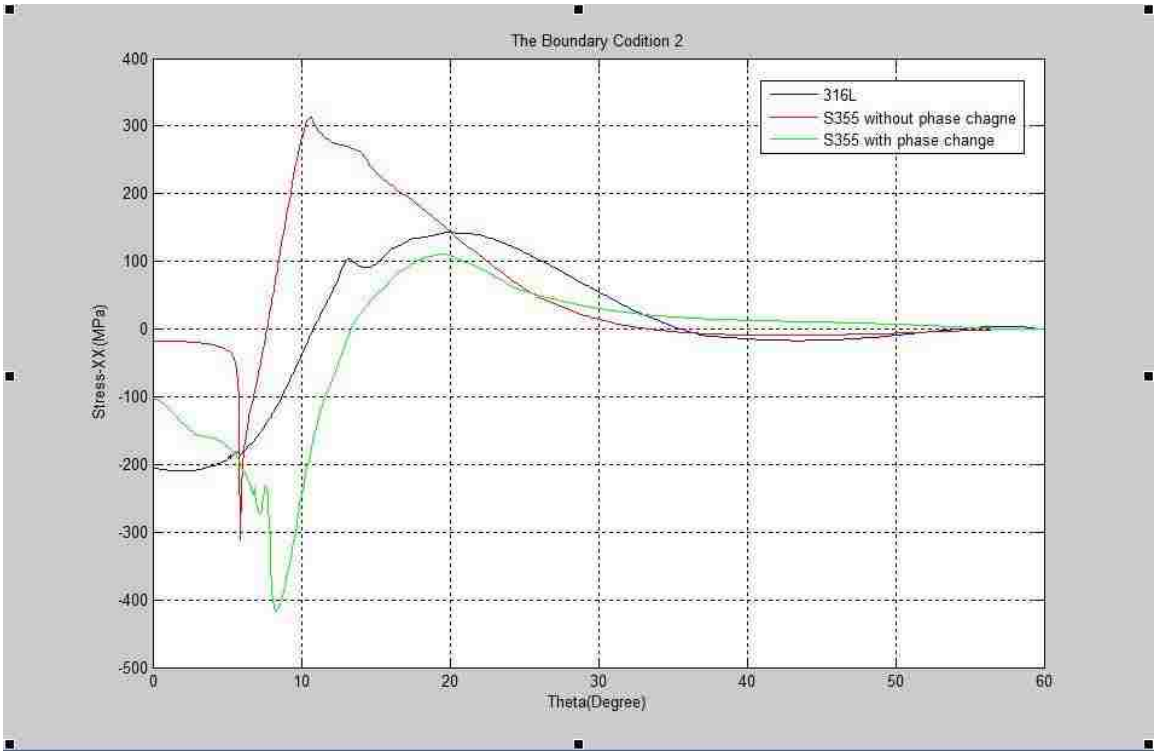

Figure 4.31 Distributions of residual stresses on top surface under boundary condition 2

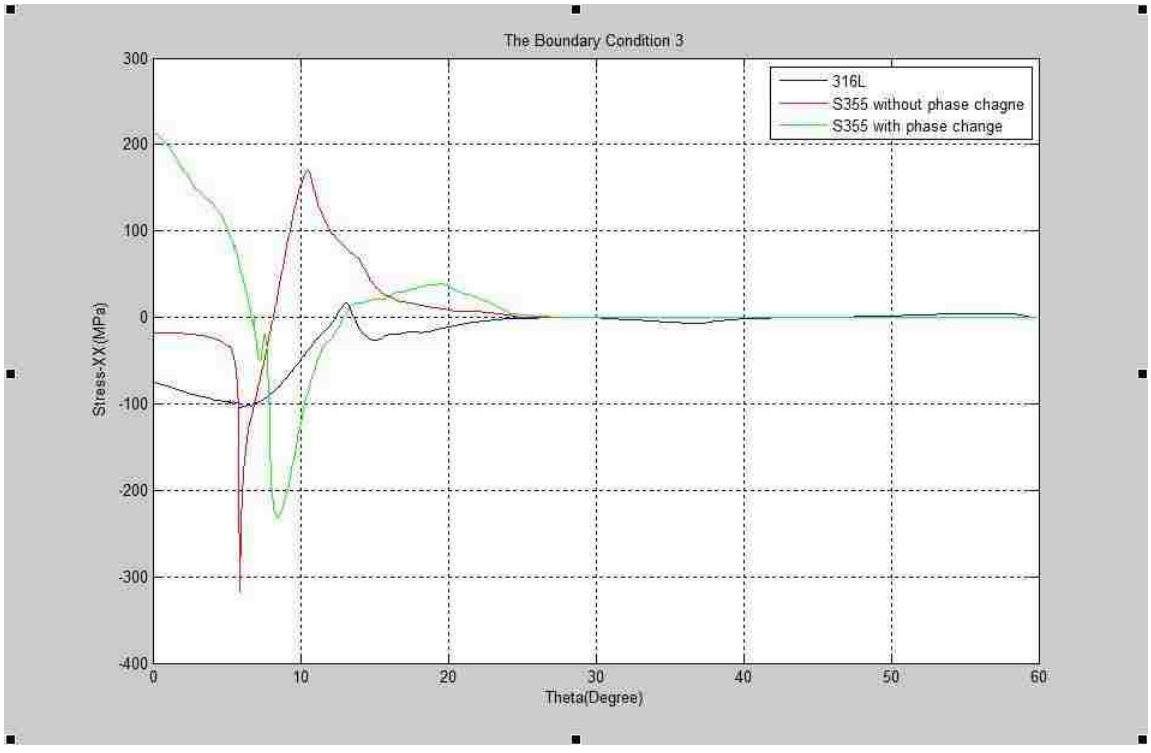

Figure 4.32 Distributions of residual stresses on top surface under boundary condition 3

Under the boundary condition 1, the unclamped condition during the entire welding process, the residual stresses σ_{rr} on the maximum radius of the welding zone of the flat plate for 316L austenitic stainless steel, S355J2G3 carbon steel with phase changes, and S355J2G3 carbon steel without phase changes are compared in Figure 4.33. The similar comparisons of the residual stresses σ_{rr} are made in Figure 4.34 for the boundary condition 2, before release of the clamped condition, and Figure 4.35 for the boundary condition 3, after release of the clamped condition. According to the analysis of these three figures, it is clear that the residual stresses σ_{rr} on the maximum radius of the welding zone of the flat plate for S355J2G3 carbon steel without phase changes during welding process are a little similar with the ones for 316L austenitic stainless steel, especially under the boundary condition 1, but are totally different from the ones for S355J2G3 carbon steel with phase changes.

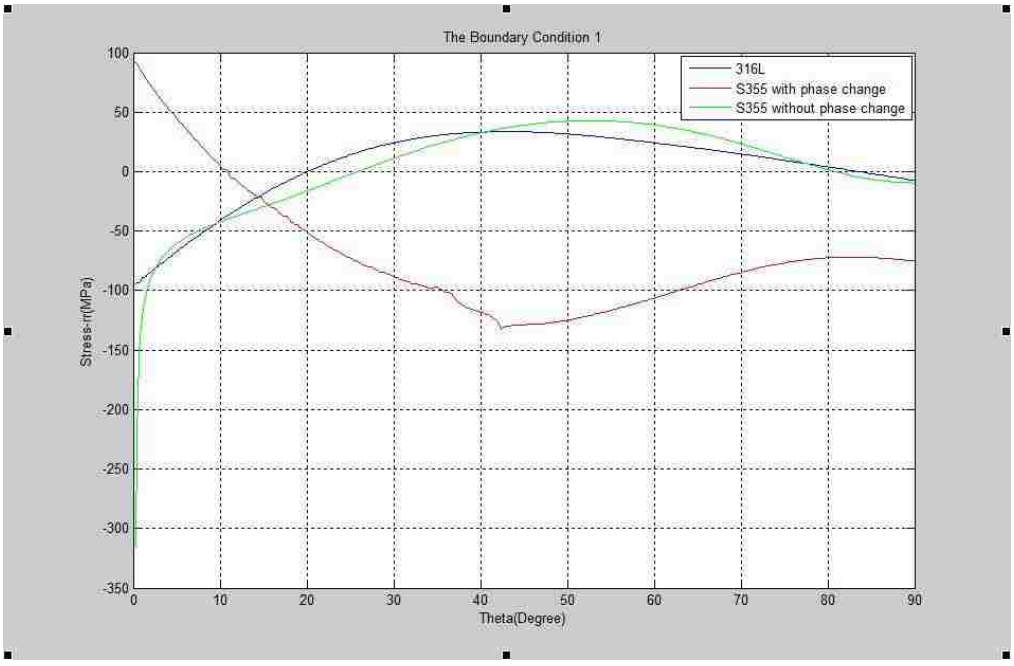

Figure 4.33 Distributions of residual tresses on maximum radius of welding zone under boundary condition 1

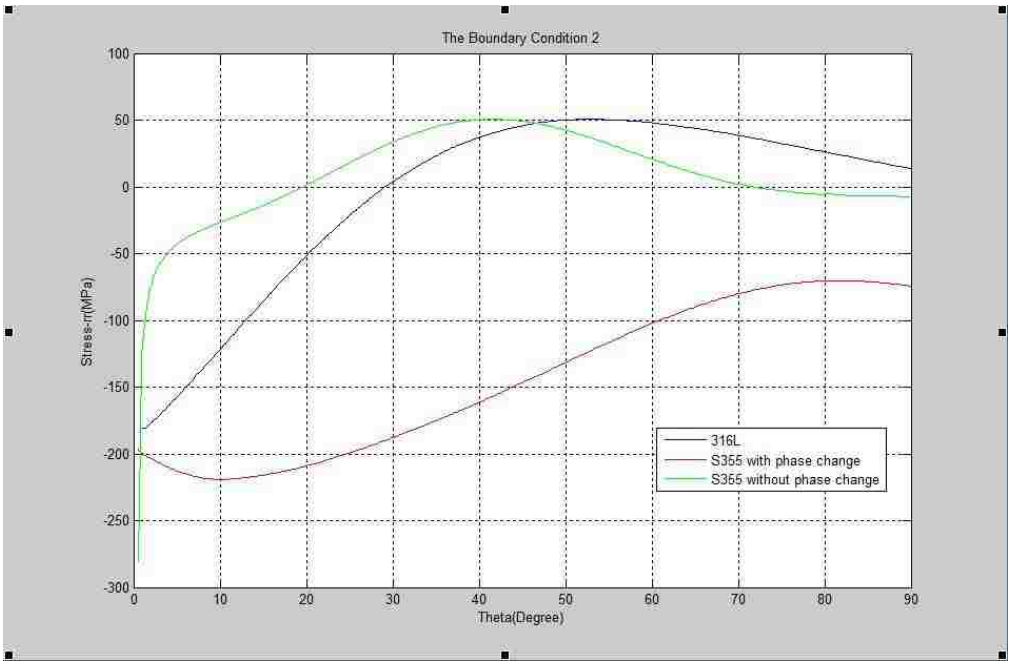

Figure 4.34 Distributions of residual tresses on maximum radius of welding zone under boundary condition 2

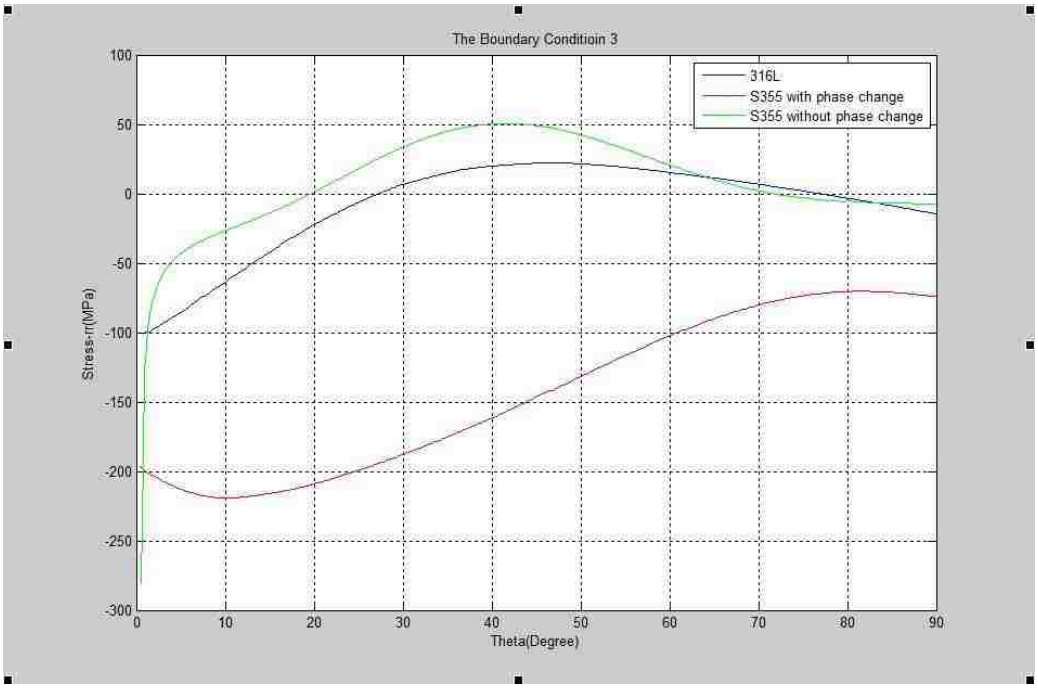

Figure 4.35 Distributions of residual tresses on maximum radius of welding zone under boundary condition 3

Chapter 5. Conclusions

During the welding process, the residual stresses will be greatly influenced by the materials, the boundary conditions, and the phase changes.

For 316L stainless steel, the boundary condition 2, before release of the clamped condition, will produce much bigger residual stresses than the other two boundary conditions, especially near the melt boundary on the top surface of the flat plate. For S355J2G3 carbon steel, the residual stresses on the top surface of the flat plate under the boundary condition 1 and 3 are very close to each other, but the boundary condition 2, before release of the clamped condition will create a bigger residual stresses near the melt boundary on the top surface.

Under the same boundary condition, the changing trends of the residual stresses on the top surface of the flat plate for 316L austenitic stainless steel and S355J2G3 carbon steel are totally different. In addition, the material, S355J2G3 carbon steel, will generate much bigger residual stresses on the top surface than 316L.

For S355J2G3 carbon steel without phase changes during welding process, the changing trends of the residual stresses on the top surface are very close to each other under the different boundary conditions, and there are the negative peak values near the melt boundary. However, under the same boundary condition, the residual stresses on the top surface of the flat plate for S355J2G3 carbon steel with phase changes and S355J2G3 carbon steel without phase changes are corresponding different.

Chapter 6. Further work

The residual stresses, σ_{yy} and σ_{xy}, on the top surface of the flat plate should be equal to zero in theory. In this study they are close to zero, but not equal to zero. In order to make the residual stresses, σ_{yy} and σ_{xy}, on the top surface of the flat plate, especially near the melt boundary, infinitely close to zero, the mesh refinement close to the melt boundary is required in the further work. In addition, the mesh refinement can make the results of the welding simulation for 316L austenitic stainless steel and S355J2G3 carbon steel more accuracy.

References

[1] Institution of Mechanical Engineers (Great Britain), Material and Mechanics of Solids Group, “RECENT ADVANCES IN WELDING SIMULAITON”, Bury St Edmunds: Professional Engineering Pub. For the Institution of Mechanical Engineers, 2000.

[2] Yukio Ueda, Hidekazu Murakawa, Ninshu Ma, “Welding Deformation and Residual Stress Prevention”, Waltham, MA: Elsevier/Butterworth-Heinemann, 2012.

[3] Jayatilaka, Ayal de S, “FRACTURE OF ENGINEERING BRITTLE MATERIALS”, London: Applied Science Publishers, 1979.

[4] H. F. Nied, D. Siegele, Study of the Influence of Material and Welding Modeling on the Residual Stresses in Longitudinal Stiffeners, COMMISSIOIN XIII FATIGUE OF WELDED COMPONENTS AND STRUCTURES XIII-2479-13, October 2013.

[5] Sindo Kou, “Welding Metallurgy (2nd Edition)”, Hoboken, N.J.: Wiley-Interscience, 2003.

[6] Theodore Kautny, “Autogenous Welding and Cutting”, New York: McGraw-Hill company, 1915.

[7] Smith, S. D., A review of numerical modelling of fusion welding for the prediction of residual stresses and distortion, TWI Report 437, December 1991.

[8] SYSWELD, User’s manual, ESI Group, 2014.

[9] SYSWELD, Engineering Simulation Solution for Heat Treatment, Welding and Welding Assembly, ESI Group, 2004.

[10] SYSWELD, Complete Finite Element Solution for Simulation of Welding Processes, ESI Group, 2003.

[11] SYSWELD, Visual-Mesh v8.0 Tutorials, ESI Group, 2012.

[12] SYSWELD, Visual-Environment OPEN & COLLABORATIVE ENGINEERING ENVIRONMENT, ESI Group, 2011.

[13] "Visual-Viewer," https://www.esi-group.com/

[14] SYSWELD, Visual-Weld v9.0 Basic/Advanced Training, ESI Group, 2013.

[15] ANSYS, User's manual, 2014.

[16] Iron and Steel Society of AIME, Product Physical Metallurgy Committee, "Austenite Formation and Decomposition", Warrendale, Pennsylvania: TMS, 2003.

[17] H. S. Khatak, Baldev Raj, "Corrosion of Austenitic Stainless Steels: Mechanism, Mitigation and Monitoring", New Delhi: Materials Park, Ohio: Narosa Publishing House, 2002.

Appendix

Listed here are the input files for the welding simulation of 316L austenitic stainless steel under the unclamped boundary condition during the entire welding process.

FLATPLATE_HT.DAT

```
NAME FLATPLATE_MESH_

SEARCH DATA 1000 ASCII


DEFINITION

 FLATPLATE

OPTION THERMAL METALLURGY  PLANE

RESTART GEOMETRY

MATERIAL PROPERTIES

 ELEMENTS GROUPS $FLATPLATE_COMPO$ / MATE 1 STATUS -10000

 ELEMENTS GROUPS $J01_WIRE$ / MATE 1 STATUS -10000

MEDIUM

 WELDLINE / GROUPS $J01_PATH$ REFERENCE $J01_REF$ ELEMENTS $J01_SEL$ START--

 $J01_SNO$ ARRIVAL $J01_ENO$ VELOCITY 6.329114 TINF 0.000 MODEL 1

$GROUP CREATE NAME GROUPNODEONLYTRAJ

NODES 98240 98241 98242 98243

$RETURN

CONSTRAINTS

 ELEMENTS GROUPS $SOL_ID_AIR_HEAT_EXCHANGE$ / KT 1 VARIABLE 1

 NODES GROUPS $GROUPNODEONLYTRAJ$ / TT 0

LOAD
```

```
1

 ELEMENTS GROUPS $SOL_ID_AIR_HEAT_EXCHANGE$ / TT 20.000

 ELEMENTS GROUPS $J01_LOAD$ / QR 1 VARIABLE -10001 TRAJECTORY 1

TABLE

 1 / FORTRAN

      function f(t)

c

c  radiative losses : f = sig * e * (t + to)(t**2 + to**2)

c

      e = 0.8

      sig = 5.67*-8

      to = 20.

      to = 20. + 273.15

      t1  = t + 273.15

      a = t1 * t1

      b = to * to

      c = a + b

      d = t1 + to

      d = d * c

      d = d * e

      d = d * sig

c
```

```
c  convective losses = 25 W/m2
      f = d + 25.
c  change to W/mm2
      d = 1*-6
      f = f * d
c
      return
      END
 10000 / FORTRAN
    FUNCTION F(X)
    DIMENSION X(4)
    F = 1
    RETURN
    END
 10001 /  FORTRAN
C
C Normalized standard ARC Power source
C
C It needs only a weldline, no reference line. It is
C axial symmetric around the weldline
C
C The total absorbed power needs to be calibrated
```

```
C with an intensity function in the welding wizzard
C or with the FIT block starting with V2008
C
C Power source dimensions see variables below
C
      FUNCTION F(X)
C
      DIMENSION X(4)
C
C Coordinates of the gauss point treated and time
C
      XX = X(1)   ; X Coordinate
      YY = X(2)   ; Y Coordinate
      ZZ = X(3)   ; Z Coordinate
      TT = X(4)   ; Time
C
C Parameters of the Goldak power source
C
C The absorbed power is defined within an ellipsoid
C
C Definition of the maximum front and rear power intensity
C
```

```
      QF = 1.0      ; Normalized maximum front power source intensity
      QR = 0.833    ; Normalized maximum rear power source intensity
C
C Definition of the measures of the Goldak ellipsoid
C They should be inside the molten zone
C
      AF = 5.333    ; Front length of the molten zone
      AR = 10.667   ; Rear length of the molten zone
C
C Width and depth
C
      B  = 6.000    ; Half of the width of the bead
      C  = 6.000    ; Penetration of the bead
C
C                   Position in space - completely handled by
C                   the welding wizzard - weldline
C
      X0 = 0.000    ; X initial location of source center
      Y0 = 0.000    ; Y initial location of source center
      Z0 = 0.000    ; Z initial location of source center
      VY = 0.0      ; Source displacement velocity
      AY = 0.000    ; Angle of torch [deg.]
```

```
C
C Computation of the absorbed power
C
C F = QC * V1 * V2 * V3 with
C V1 = exp( -( YY-Y0-VY*TT )^2/AC^2 )
C V2 = exp( -( XX-X0 )^2/B^2 )
C V3 = exp( -( ZZ-Z0 )^2/C^2 )
C if ( -YY + Y0 +VY*TT ) greater than 0
C   QC = QF et AC = AF
C else
C   QC = QR et AC = AR
C
C Constant
C
      M1 = -1
      PIDEG = ATAN(1.)
      PIDEG = PIDEG / 45.
      AY = AY * PIDEG
C
C Transformation of global to local coordinates
C
      XD   = XX - X0
```

```
      YD   = VY * TT
      YD   = YD + Y0
      ZD   = ZZ - Z0
C
C Source rotation about Y axis
C
      SA   = SIN( AY )
      SA   = - SA
      CA   = COS( AY )
      A1   = XD * CA
      A2   = ZD * SA
      XL   = A1 + A2
      YL   = YY - YD
      A1   = ZD * CA
      A2   = XD * SA
      ZL   = A1 - A2
C
C Condition computation, QC and AC initialisation
C
      COND = VY * YL
      IF (VY .EQ. 0.) COND = YL
      QC   = QR
```

```
      AC   = AR
      IF( COND .GT. 0. ) QC = QF
      IF( COND .GT. 0. ) AC = AF
C
C Vi computation
C
      A1   = YL * YL
      A2   = AC * AC
      A2   = A1 / A2
      A2   = M1 * A2
      V1   = EXP( A2 )
C
C V2 computation
C
      A1   = XL * XL
      A2   = B * B
      A2   = A1 / A2
      A2   = M1 * A2
      V2   = EXP( A2 )
C
C V3 computation
C
```

```
      A1   = ZL * ZL

      A2   = C * C

      A2   = A1 / A2

      A2   = M1 * A2

      V3   = EXP( A2 )

C

C F computation

C

      F    = QC * V1

      F    = F * V2

      F    = F * V3

C

      RETURN

      END

RETURN



NAME FLATPLATE_

SAVE DATA 1000
```

FLATPLATE_MECH.DAT

NAME FLATPLATE_MESH_

SEARCH DATA 1000 ASCII

DEFINITION

FLATPLATE

OPTION TWO-DIMENSIONAL TRANSLATION THERMOELASTICITY

RESTART GEOMETRY

MATERIAL PROPERTIES

ELEMENTS GROUPS $FLATPLATE_COMPO$ / E -10000 NU 0.3 LX -10001 LY -10001 --

LZ -10001 YIELD -10002 SLOPE -10003 PHAS 2 TF 1400 AUST 2 KY -1 MODEL 3 --

STATUS -10004

ELEMENTS GROUPS $J01_WIRE$ / E -10000 NU 0.3 LX -10001 LY -10001 LZ -10001 --

YIELD -10002 SLOPE -10003 PHAS 2 TF 1400 AUST 2 KY -1 MODEL 3 STATUS -10004

MEDIUM

WELDLINE / GROUPS $J01_PATH$ REFERENCE $J01_REF$ ELEMENTS $J01_SEL$ START--

$J01_SNO$ ARRIVAL $J01_ENO$ VELOCITY 6.329114 TINF 0.000 MODEL 1

$GROUP CREATE NAME GROUPNODEONLYTRAJ

NODES 98240 98241 98242 98243

$RETURN

CONSTRAINTS

```
 NODES GROUPS $RIGID01_CLAMP$ / UX

 NODES GROUPS $RIGID03_CLAMP$ / UX UY UZ

 NODES GROUPS $GROUPNODEONLYTRAJ$ / UX UY UZ

LOAD

1 / NOTHING

TABLE

 10000 / -10005 -10006

 10001 / -10007 -10008

 10002 / -10009 -10010

 10003 / -10011 -10011

 10004 / FORTRAN

   FUNCTION F(X)

   DIMENSION X(4)

   F = 1

   RETURN

   END

 10005 / 1  20 192372 100 185860 200 177720 300 169580 400 161440 500 153300

 600 145100 700 137020 800 109766 900 63195 1000 37367 1100 16418

 1200 10836 1300 8532 1400 859

 10006 / 1   20 1000    1500 1000

 10007 / 1  20 0 100 0.00123 200 0.00292 300 0.00472 400 0.0066 500 0.00853

 600 0.0105 700 0.0125 800 0.0146 900 0.0167 1000 0.0189 1100 0.0211
```

1200 0.0234 1300 0.0256 1400 0.0279

10008 / 1 0 0 1500 0

10009 / 1 20 275 100 238 200 198 300 172 400 157 500 151 600 145 700

136 800 127 900 115 1000 78 1100 38 1200 24 1300 16 1400 2

10010 / 1 20 275 100 238 200 198 300 172 400 157 500 151 600 145 700

136 800 127 900 115 1000 78 1100 38 1200 24 1300 16 1400 2

10011 / 7 20 10012 100 10013 200 10014 300 10015 400 10016 500 10017

600 10018 700 10019 800 10020 900 10021 1000 10022 1100 10023 1200 10024 1300 10025 1400 10026

10012 / 1 0 0 0.2 286

10013 / 1 0 0 0.2 252

10014 / 1 0 0 0.2 269

10015 / 1 0 0 0.2 279

10016 / 1 0 0 0.2 278

10017 / 1 0 0 0.2 268

10018 / 1 0 0 0.2 242

10019 / 1 0 0 0.2 204

10020 / 1 0 0 0.2 166

10021 / 1 0 0 0.2 54

10022 / 1 0 0 0.2 22

10023 / 1 0 0 0.2 6

10024 / 1 0 0 0.2 5

10025 / 1 0 0 0.2 7

10026 / 1 0 0 0.2 0.1

RETURN

NAME FLATPLATE_

SAVE DATA 2000

MEDIUM

EXTRACT MEDIUM

VITA

Bin Yang was born on March 13, 1987 in Shengfang, Hebei Province in P. R. China. He has been at Lehigh University since 2012 as a graduate student in Department of Mechanical Engineering and Mechanics.